

# Quantum computing for discrete optimization: a highlight of three technologies.

Alexey Bochkarev<sup>\*1</sup>, Raoul Heese<sup>2</sup>, Sven Jäger<sup>1</sup>, Philine Schiewe<sup>3</sup>, and  
Anita Schöbel<sup>1,2</sup>

<sup>1</sup>Department of Mathematics, RPTU Kaiserslautern-Landau, Kaiserslautern, 67663, Germany

<sup>2</sup>Fraunhofer Institute of Industrial Mathematics ITWM, Kaiserslautern, 67663, Germany

<sup>3</sup>Department of Mathematics and Systems Analysis, Aalto University, Espoo, 02150, Finland

September 2, 2024

Quantum optimization has emerged as a promising frontier of quantum computing, providing novel numerical approaches to mathematical optimization problems. The main goal of this paper is to facilitate interdisciplinary research between the operations research (OR) and quantum computing communities by providing an OR scientist’s perspective on selected quantum-powered methods for discrete optimization. To this end, we consider three quantum-powered optimization approaches that make use of different types of quantum hardware available on the market. To illustrate these approaches, we solve three classical optimization problems: the Traveling Salesperson Problem, Weighted Maximum Cut, and Maximum Independent Set. With a general OR audience in mind, we attempt to provide an intuition behind each approach along with key references, describe the corresponding high-level workflow, and highlight crucial practical considerations. In particular, we emphasize the importance of problem formulations and device-specific configurations, and their impact on the amount of resources required for computation (where we focus on the number of qubits). These points are illustrated with a series of experiments on three types of quantum computers: a neutral atom machine from *QuEra*, a quantum annealer from *D-Wave*, and a gate-based device from *IBM*.

## 1. Introduction

Discrete optimization is central to many problems in operations research (OR), often arising in efficient organization of complex systems across various domains: logistics, supply chain management, transportation, finance, healthcare, and more. This led to the development of a vast variety of computational methods, with many state-of-the-art algorithms already incorporated into advanced stand-alone solvers, such as Gurobi (Gurobi, 2024), SCIP (Bolusani et al., 2024), and others. Still, in practice such problems often require significant amount of resources, as the solution space grows exponentially with the problem size.

Quantum computing offers an alternative computation model, but both the methodology and the hardware are in early stages of development, as compared to classical computing. It is not clear to what extent, if at all, OR will benefit from quantum technology. There are reasons to believe that it might yield a significant speed-up, especially for discrete optimization (Preskill, 2018), although no practical (exponential) quantum advantage has yet been demonstrated for an optimization problem (Hoeffler et al., 2023). We think that to be able to assess potential opportunities at this early stage,

---

\*The work was partially supported by the Research Initiative Quantum Computing for Artificial Intelligence (QC-AI).

OR experts might want to familiarize themselves with the topic to a certain degree. However, the necessary background knowledge significantly differs from a typical discrete optimization specialist training. This is mainly because the language used in the literature naturally draws on the works from quantum physics, making it less accessible to the general mathematical readership.

A discussion of possible synergies between OR and quantum information science along with further research directions is presented by Parekh (2023); Klug (2024); Au-Yeung et al. (2023). A comprehensive overview of quantum optimization is provided by Abbas et al. (2023). The current state and prospects of quantum computers (QCs) are discussed by Scholten et al. (2024). There is also a significant body of literature devoted to numerical investigation and benchmarking of different quantum-powered approaches (Lubinski et al., 2024).

This paper fundamentally differs from the overviews mentioned above. Instead of giving a broad high-level overview, we focus on a selection of specific quantum devices and types of discrete optimization problems, and seek to achieve three goals: convey a high-level intuition behind each of the approaches, provide the references necessary for a more precise understanding, and discuss the relevant workflows and key practical considerations. Our findings highlight the fact that the number of qubits required to solve an optimization problem depends not only on the number of binary variables, but also on the problem structure, formulation, and the specific quantum device. We illustrate these aspects with a series of experiments.

The paper is structured as follows. In the next section, we focus on the motivation for applying quantum computing to discrete optimization. Section 3 presents three selected quantum technologies, focusing on their workflows for optimization. Then, in Section 4 we discuss the application of these workflows to three specific discrete optimization problems, highlighting the necessary number of qubits in connection to the chosen computational approach. This discussion is further illustrated with numerical results presented in Section 5. Section 6 concludes with a summary and a brief outlook.

## 2. Quantum optimization

A quantum computer is a computational device that harnesses quantum physics to process information in fundamentally new ways (Nielsen & Chuang, 2010). This makes it a potentially powerful tool for solving optimization problems. At present, however, improvements on both the algorithmic and the hardware side are still needed to realize an advantage for practical applications (Abbas et al., 2023). In the following, we briefly outline how QCs work and motivate their use for optimization tasks in light of the technologies that are the focus of this paper.

### 2.1. Quantum computing

The quantum processing unit (QPU) is the core processing unit within a QC in analogy to the central processing unit (CPU) within a conventional computer. Practically usable QPUs include superconducting devices (e.g., by IBM, D-Wave, Google, IQM, and Rigetti), photonic devices (e.g., by Xanadu), neutral atom devices (e.g., by QuEra, Pasqal, and RymaxOne), and trapped ion devices (e.g., by Quantinuum, Honeywell QS, and IonQ), just to name a few (Gyongyosi & Imre, 2019).

The key components of a QPU, quantum bits or *qubits*, exhibit more complex behavior than classical bits. When we read a classical bit, we always get a definite answer, 0 or 1. That is, a classical bit is always either in the state 0 or in the state 1. In contrast, qubits can not only attain the states 0 (which is also called the *ground state*) and 1 (which is also called the *excited state*), but also a *superposition* state of 0 and 1. Measuring a qubit in such a superposition state yields inherently random results: we get 0 or 1 with certain probabilities. This randomness is not the result of technical limitations, but an intrinsic property of quantum physics (Bera et al., 2017). Furthermore, quantum measurements are inherently destructive in the sense that the superposition of the qubit (i.e., the information concerning the respective probabilities before the measurement) is irrevocably lost after the measurement process.

Not only is information stored and measured differently in a QC, but the interactions between qubits are also more complex than the interactions between classical bits. It is this complex interaction of multi-qubit systems that makes QCs potentially powerful. A multi-qubit system can attain a so-called *entangled* state, meaning that operations on one qubit can affect other qubits, which is a key feature

used in quantum algorithms and leads to a correlation of the (inherently random) measurement results of different qubits. As a consequence, the measurement results of an  $n$ -qubit system can be viewed as samples drawn from a joint probability distribution with a number of parameters exponential in  $n$ . This may (or may not) address the limitations of classical systems in some cases, when an exponentially large state space leads to practical intractability of the problem at hand. Entangled multi-qubit systems enable *quantum parallelism*, which is not equivalent to mere parallel computation, as different branches of computation can actually interact, an effect also known as *interference* (Markidis, 2024). As a prototypical example, the Deutsch-Josza algorithm (Nielsen & Chuang, 2010) determines a global property of a Boolean function using a single quantum evaluation.

On the flip side, the unique computational model of QCs also entails new difficulties to designing efficient algorithms. For example, the inherent randomness of measurements requires an algorithmic design that can operate on finite samples (i.e., measurement results) of the underlying joint probability distribution. Moreover, a practical challenge also lies in the hardware. QCs are currently very error-prone and have extremely limited resources, which is why they are also sometimes called noisy intermediate scale quantum (NISQ) devices. Algorithms must take these hardware-induced errors and limitations into account. Therefore, brute-force implementations of classical algorithms on QCs usually do not lead to performance gains (in fact, the opposite is true). Specialized solutions for carefully selected problem classes are needed to make the most of the hardware (Harrow & Montanaro, 2017). In this sense, a QPU is similar to a graphical processing unit (GPU), as it is also a specialized processor that fits well for very specific tasks. To alleviate these NISQ limitations, so-called *hybrid quantum-classical algorithms* can be used, where quantum and classical computations are performed together. The QPU can then be used to solve only the specific tasks for which it is suitable. We present an example for such approach in Section 3.3.

There are generally two modes of operation for a QPU: analog and digital. In *analog mode*, computations are realized with a continuous control of the quantum system, similar to how quantum systems behave in nature due to the laws of quantum physics. The *digital mode*, on the other hand, is based on discrete controls, so-called *gates* (in analogy to classical logical gates, such as AND or XOR), which is why this mode of operation is also referred to as gate-based quantum computing (GQC). Gates are effectively a discretization of the underlying continuous controls, making the digital mode an additional level of abstraction compared to the analog mode. We will consider a few technologies in Section 3 illustrating both these modes of operation.

## 2.2. Quantum advantage

Although quantum computing clearly offers novel approaches, it has not yet been proven that it can currently enable superpolynomial speedups for practically relevant discrete optimization problems (Abbas et al., 2023). However, quantum optimization remains a very active field of research with constant improvements. Preskill (2018) formulated three main reasons to think that a “quantum advantage” could one day be realized.

1. There are examples of mathematical problems that are believed hard to solve for classical computers, and for which efficient quantum-powered algorithms exist (e.g., factoring integers and finding discrete logarithms, see Shor, 1997).
2. There are quantum states that are relatively easy to prepare on a QC such that measuring them is equivalent to the sampling of random numbers from a particular probability distribution, which is impossible to achieve efficiently by classical means (Harrow & Montanaro, 2017).
3. No efficient classical algorithm is known that would be able to simulate a QC efficiently at arbitrary scales, which is essentially due to the exponentially large state space of a multi-qubit system.

It is not immediately obvious how these points translate to practical applications in the OR context. However, they do justify the interest in quantum computing research, and, in particular, the search for practical ways to tackle hard discrete optimization problems using QCs.

### 2.3. Adiabatic evolution

The quantum-powered optimization approaches we consider in this paper are all inspired by so called quantum adiabatic algorithms (QAAs) (Farhi et al., 2000; Albash & Lidar, 2018) and the central idea of solving optimization problems by exploiting the natural behavior of quantum systems. On an abstract (hardware-agnostic) level, the approach can generally be described as follows.

The process starts by initializing the quantum system in a simple minimum energy state (the ground state), which is known and easy to prepare. In particular, it is completely independent from the optimization problem of interest. Over time, the system is slowly tuned (or “evolved”) by gradually controlling the underlying system properties that govern the quantum dynamics, performing the appropriate quantum state manipulations. Altering the quantum state can also be considered as altering the energy landscape of the system: the energy levels that can be associated with its different states. In this sense, the goal of the controlled evolution is to gradually shape an energy landscape to match the optimization landscape of the problem of interest. In particular, after a carefully performed evolution process, a minimum energy state of the multi-qubit system of the QPU reflects an optimal solution to the optimization problem.

The *adiabatic theorem* of quantum physics guarantees that, if the changes to the system are made slowly enough (we will revisit this topic further below), the system will remain in its lowest energy state. As the landscape adjusts, its energy minimum might shift, and correspond to another state of the qubits, but the system is able to naturally “slide” to a global minimum energy state of the tuned system, resulting in the desired answer. Moreover, due to the physical effect called *tunneling*, the system has chances of escaping local optima in the process. Measurement of the qubits then reveals a candidate solution to the optimization problem of interest, in form of a bitstring with one bit as the measurement result for each qubit. The surprising insight is that it is not necessary to know how to solve the optimization problem to be able to prepare a state that contains this information. It is only possible because quantum physics itself is used to discover the solution in the sense of an analog computation.

The necessary pace of the changes in the system (so that it would be “slow enough”) depends on the size of so-called *minimum energy gap*, the smallest energy difference between the ground state and the second lowest energy state throughout the entire evolution process. The time evolution of a quantum state that complies with the adiabatic theorem is also called *adiabatic evolution*. Therefore, in the QAA process, the system is made to evolve adiabatically from the trivial initial state to a problem-specific final state. By construction, this final state is again a ground state and hence the measurement reveals a solution.

Typically, the final state is a superposition state such that repeating the entire process might yield different solution candidates from new measurements. In a theoretically perfect scenario, these solution candidates would all be optimal solutions to the underlying problem (each with the same minimal energy). In practice, however, quantum fluctuations, an insufficiently slow evolution speed (due to the lack of knowledge about the minimum energy gap, which can only be determined when the optimal solution of the optimization problem is already known in advance), and hardware-related uncertainties of NISQ devices lead to a final state that is in a superposition of sub-optimal (and potentially optimal) solutions. In other words, measuring the final state may reveal sub-optimal solutions, making the algorithm effectively a heuristic. It is therefore common to collect data from multiple algorithm runs, usually referred to as *shots*, to choose the best outcome.

QAA is inherently different from classical methods because it relies on the quantum property of superposition, which allows the system to explore many possible solutions “simultaneously”. As a consequence, quantum adiabatic algorithms have the potential to outperform classical approaches. However, this presumption has not been demonstrated for problems of practical scale yet, and is the subject of ongoing research.

## 3. Quantum optimization workflows

To illustrate different QPUs and different QAAs, we consider the following three alternative quantum-powered approaches in this paper, each having certain “natural” input problem formulation.

Table 1: Quantum-powered optimization approaches, each based on a different QPU technology from a different provider.

Approach	Hardware	Mode	Provider	Algorithm	Problem class	Section
NA-OPT	Neutral atoms	analog	<i>QuEra</i>	QAA	UD-MIS	<a href="#">3.1</a>
QA-OPT	Superconducting	analog	<i>D-Wave</i>	QA	QUBO	<a href="#">3.2</a>
QAOA-OPT	Superconducting	digital	<i>IBM</i>	QAOA	QUBO	<a href="#">3.3</a>

1. Solving maximum independent set problems on unit disk graphs (UD-MIS) with the neutral atoms based device *Aquila* from *QuEra* (Wurtz et al., 2023) in analog mode. It can be accessed commercially online via the *AWS Braket* cloud service (Amazon Web Services, 2020). This approach is in the following referred to as NA-OPT.
2. Solving quadratic unconstrained binary optimization problems (QUBOs) with the *D-Wave Advantage* quantum annealer (McGeoch & Farré, 2020), an analog device, which is commercially accessible online via the *Leap* cloud service (D-Wave, 2024). This approach is in the following referred to as QA-OPT.
3. Solving QUBOs with superconducting gate-based computers from *IBM*, which are commercially accessible online via the *IBM Quantum* cloud service (IBM Quantum, 2023a). This approach is in the following referred to as QAOA-OPT.

A summary of the three approaches is also listed in Table 1. We discuss specific problem formulations in detail in Section 4. The three approaches share a unified workflow that includes three common high-level steps, as sketched in Figure 1:

- (I) Modeling: To begin with, the given problem  $P$  has to be *modeled*, depending on the chosen QPU and the computational approach.
- (II) Configuration: During the second step, this device-specific problem formulation is used to specify the model-dependent *configuration* of the QPU. It involves setting up algorithm parameters that are independent of the specific device at hand, as well as device-dependent configuration, which we discuss further for each QPU separately.
- (III) Solution: Finally, the actual *solution* takes place in step three, usually involving a series of QPU shots and additional classical computations, (e.g., pre- and post-processing).

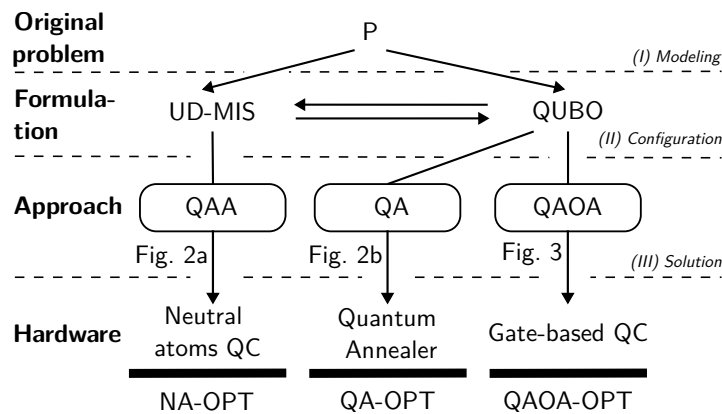


Figure 1: Each of the three central columns represent the workflow for one of the quantum-powered optimization approaches from Table 1.

In the following, we provide a brief outline of the three approaches in the context of these three high-level steps. We limit ourselves to description of the fundamental principles and refer to the provided references for more details.

### 3.1. NA-OPT: solving UD-MIS with an analog QC

Our first approach, NA-OPT, makes use of the neutral atom device *Aquila* from *QuEra* (Wurtz et al., 2023) in analog mode to solve UD-MIS (Pichler et al., 2018; Ebadi et al., 2021, 2022) by exploiting the so-called *Rydberg blockade effect*, a physical law originating from quantum physics. A recent review of the technology is given by Wintersperger et al. (2023).

**Hardware.** In the *Aquila* device, qubits are physically realized by rubidium atoms, which are trapped in a vacuum cell by lasers and can be arranged on a two-dimensional plane using optical tweezers. The atoms can be utilized as so-called *Rydberg qubits*, which possess two basis states: the non-excited (or ground) state and the excited (Rydberg) state. The Rydberg blockade effect makes it energetically favorable that atoms within a certain distance from each other, the so-called *Rydberg blockade radius*, are not excited simultaneously. This effect can be used to solve UD-MIS, as explained in the following.

**Algorithm.** Presuming nodes that are localized on an Euclidean plane, a unit disk graph has the property that there is an edge between two vertices if and only if the corresponding vertices are within a unit distance of each other. In other words, the relative location of nodes determines their connectivity. Given the unit disk graph from the UD-MIS, we associate an atom with each node and arrange the atoms on the two-dimensional plane according to the corresponding (scaled) node coordinates to achieve a one-to-one spatial correspondence between graph nodes and atoms. The Rydberg blockade radius of the system is tuned to match the unit disk radius such that atoms that correspond to connected nodes lie within the Rydberg blockade radius. As a consequence, the ground state of the quantum system encodes a UD-MIS solution: the atoms in the excited state indicate the resulting node set.

With this problem encoding, a QAA can be realized by evolving the system in a controlled fashion with external laser fields. To this end, we start from a problem-agnostic minimum energy state, and slowly adjust the controls to arrive at a problem-specific minimum energy state while the positions of the atoms remain unchanged. This way, an atom in the excited state indicates that the corresponding node belongs to the candidate solution, and the ground state indicates otherwise. The Rydberg blockade effect is intended to ensure the constraints of the optimization problem, which require that neighboring nodes cannot both be part of the resulting node set. Without it, the minimum energy state would simply correspond to an excitation of all atoms.

For the end user, the computations described above follow the generic quantum computing protocol from Section 3, a device-specific scheme is summarized in Figure 2a.

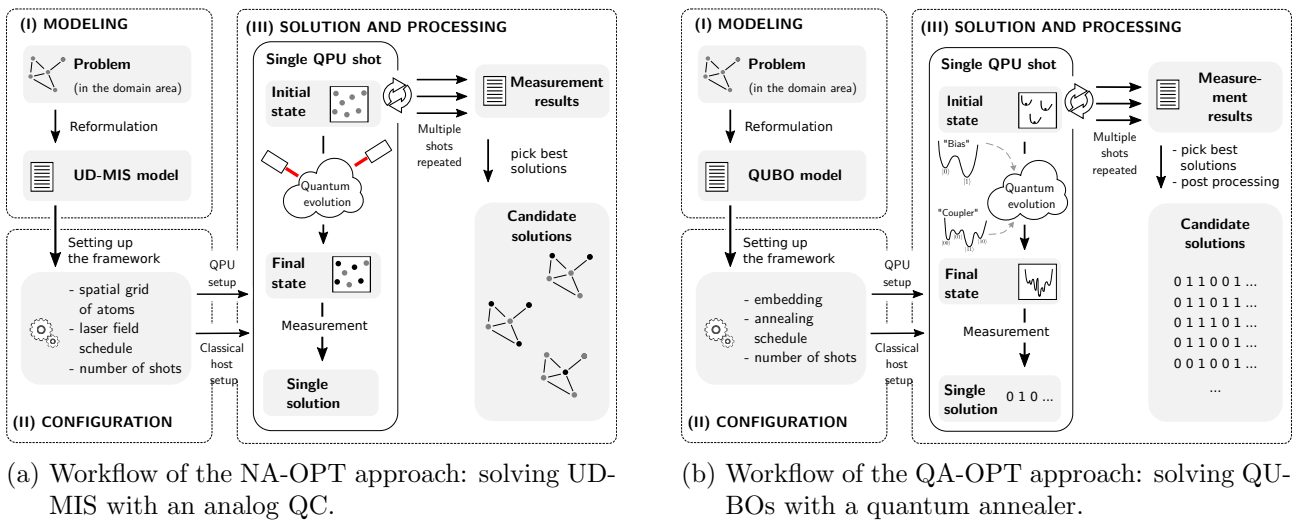


Figure 2: Workflows for two analog QPUs.

Serret et al. (2020) estimate the necessary size of a neutral atom array to yield an advantage over classical approximation algorithms for UD-MIS, and Wurtz et al. (2022) provide an overview of the

connections between the maximum independent set and many OR problems in this context. Note, however, that neutral atom arrays can be used to solve other problem classes as well, it is an active field of research (Nguyen et al., 2023). For instance, a conceptual idea for a non-unit disk (non-blockade-based) framework was suggested by Goswami et al. (2024).

Finally, let us highlight a few practical issues related to this approach. First, the geometric configurations of the atoms array, and hence possible input configurations, are restricted to a square two-dimensional lattice of effective size at most  $75\ \mu\text{m} \times 76\ \mu\text{m}$  with the minimum distance between the atoms being about  $4\ \mu\text{m}$ . Second, the Aquila device can only hold up to 256 atoms in the array at once, which translates to at most 256 nodes in the UD-MIS instance.

Using a hardware feature called local detuning, Aquila can also be used to solve maximum-weight independent set problem on unit disk graph (UD-MWIS) problems in complete analogy to UD-MIS. However, at the time of performing the experiments, this extension was not supported yet and we therefore limit ourselves to UD-MIS in the numerical experiments.

**Number of qubits needed.** As the decision version of the UD-MIS problem is  $\mathcal{NP}$ -complete (Clark et al., 1990), reducing an arbitrary problem from  $\mathcal{NP}$  to it is possible with a polynomial overhead in the instance size. It might be possible to transform a QUBO to UD-MIS instance using fewer nodes (and hence, qubits), but we will focus on the following general result: Nguyen et al. (2023) proposed a transformation that maps a QUBO instance with  $n$  variables to an equivalent maximum-weight independent set problem (MWIS) over a unit disk graph with at most  $4n^2$  nodes. These qubit requirements are summarized in Lemma 1.

**Lemma 1.** (Nguyen et al., 2023, Section V.C) *An arbitrary UD-MIS instance with  $n$  nodes can be solved on a neutral atom computer with  $n$  qubits. An arbitrary QUBO instance with  $n$  binary variables can be encoded as a UD-MWIS with at most  $4n^2$  nodes, and hence, requires a neutral atom computer with  $4n^2$  physical qubits.*

Here and in the following, we use the term *logical qubits* when we refer to the abstract concept of qubits disregarding a specific hardware implementation and *physical qubit* to denote the physical implementation of a qubit within a specific device (e.g., an atom).

### 3.2. QA-OPT: solving QUBOs with a quantum annealer

Our second approach, QA-OPT, makes use of the *Advantage* quantum annealer from *D-Wave* (McGeoch & Farré, 2020) to solve QUBOs. Note that Advantage is a special-purpose device designed to solve this type of problems.

**Hardware.** The system is based on superconducting technology. Qubits are physically realized using specialized components based on superconducting loops and qubit manipulations are implemented via so-called couplers and biases. The *bias* of each qubit makes it more energetically favorable for this qubit to end up in a specific state (either the ground, or the excited state). A *coupler* controls the interaction between two qubits: It is implemented as another electric circuit that physically interacts with both qubits' loops via electro-magnetic fields. It allows to increase or decrease the energy of the system corresponding to the states where these two qubits yield the same measurement results. For technical reasons, couplers are only implemented between physically adjacent qubits, which means that there is a limit to the interactions that can be realized. We will revisit this topic further below.

**Algorithm.** The operation principle of the annealer is conceptually a QAA. Presume that each variable of a given QUBO is represented by a single qubit. The system is initially prepared in a problem-agnostic minimum energy state, a balanced superposition state of every qubit, for which an immediate measurement would return a uniformly random candidate solution. Then, using biases and couplers, a problem-specific minimum energy state is approached that encodes the candidate solution. In other words, the biases and couplers are tuned to represent the QUBO coefficients. A solution candidate can then be obtained from a measurement of the final state. This annealing process is typically repeated multiple times to generate an ensemble of solutions.

The device-specific workflow for the end user is shown in Figure 2b, it follows the generic quantum computing protocol from Section 3. In the first step, the optimization problem of interest is to be reformulated as a QUBO. The second step is to specify the problem-specific target system configuration and the evolution parameters. Finally, the actual quantum annealing takes place, each shot returning a bitstring that corresponds to a single QUBO solution candidate.

There are three key issues related to the practical usage of the Advantage device. First, the adiabatic theorem requires a sufficiently slow state transition (depending on the minimum energy gap), but the hardware-related noise increases with longer annealing times. Therefore, a compromise between these two factors of influence has to be found. Second, similar to the neutral atom computer, a QUBO with  $n$  variables can require more than  $n$  physical qubits, as discussed further. Third, biases and couplers have a limited effective resolution, which means that a QUBO can only be represented efficiently if its coefficients have a limited dynamic range (the ratio between largest and smallest values; see Mücke et al. 2023).

**Number of qubits needed.** The task of encoding a QUBO on the device can in fact be a challenging problem by itself. It requires to map QUBO variables, corresponding to logical qubits, to physical qubits.

As already mentioned above, the Advantage device only supports couplers between specific qubits, which means that the embedding of a sufficiently large and dense QUBO might require non-existing couplers. To overcome this limitation, a QUBO variable can also be encoded as a *chain* comprising several physical qubits (Venegas-Andraca et al., 2018) that are strongly coupled with each other. This corresponds to the graph-theoretic problem of finding a *minor embedding* (Choi, 2008) of the *problem graph* (where nodes are QUBO variables and edges correspond to nonzero cost coefficients) into the *topology graph* of the QPU (nodes are physical qubits, edges exist for every coupler). In this context, the chains are usually called the *branch sets* of the nodes of problem graph. If possible, chains are to be avoided because *chain breaks* are an important type of errors occurring in quantum annealers, where physical qubits representing the same logical qubit within the chain attain different states. Some *post-processing* techniques to recover consistent solutions have been proposed (Pelofske et al., 2020).

The Advantage device is designed after the so-called *Pegasus* topology (Dattani et al., 2019; Boothby et al., 2020) of 5,640 qubits, with the caveat that certain qubits might be broken as a result of hardware faults, so that the actual topology graph is a subgraph of the regular Pegasus graph. Deciding whether a given problem graph is a minor of such irregular topology graph is  $\mathcal{NP}$ -complete (Lobe & Lutz, 2024). Therefore, in practice the embedding problem is usually solved heuristically (Cai et al., 2014; Zbinden et al., 2020). These heuristics aim to find embeddings that use few physical qubits while maintaining some redundancy to strengthen the coupling of the chains and reduce the probability of errors (Pelofske, 2024). However, here we only focus on embeddings into the perfect (i.e., defect-free) Pegasus topology, and the following lemma provides a bound on the number of physical qubits required. (See Appendix G for more details.)

**Lemma 2.** *A problem graph  $G_Q$  corresponding to an arbitrary QUBO instance with  $n$  variables can be embedded into a Pegasus graph  $G_T$  with*

$$N_{QA}(n) := 24 \left\lceil \frac{n+10}{12} \right\rceil \left\lceil \frac{n-2}{12} \right\rceil \leq \frac{(n+21)(n+9)}{6}$$

*nodes corresponding to physical qubits. Therefore, an arbitrary QUBO with  $n$  variables can be solved on a quantum annealer with Pegasus topology of  $N_{QA}(n)$  qubits. If the QUBO graph  $G_Q$  is a subgraph of the Pegasus graph,  $n$  qubits suffice.*

Note that in the present approach and the one from Section 3.1, the same QUBO problem with the same number of binary variables may require different numbers of physical qubits depending on the problem structure and device implementation details. We will discuss this issue in more detail in Section 4.



### 3.3. QAOA-OPT: solving QUBOs with gate-based QCs

Our third approach, QAOA-OPT, makes use of the gate-based QCs from *IBM* to solve QUBOs. *IBM* provides a collection of QPUs, each consisting of superconducting transmon qubits contained in dilution refrigerators. For our numerical experiments, we have made use of two of the 127-qubit devices: *ibm\_cusco* and *ibm\_nazca*.

**Hardware.** The *IBM* devices are universal gate-based QCs. As such, they can run any quantum algorithm, which typically requires three steps. First, all qubits are prepared in the ground state. Then, a sequence of gates is applied, each altering the quantum state of the multi-qubit system. Finally, a measurement of the resulting state yields an outcome. A shot consists of performing all of these steps to get a single bitstring. A sequence of gates acting on a set of qubits is also referred to as a *quantum circuit* and provides all necessary instructions to operate a gate-based QC. In other words, a quantum circuit controls the evolution from an initial quantum state to a final quantum state, which is then measured.

**Algorithm.** We consider the quantum approximate optimization algorithm (QAOA) (Farhi et al., 2014; Grange et al., 2023; Blekos et al., 2024) for the solution of QUBOs, which is a hybrid quantum-classical algorithm that can be understood as an attempt to digitize adiabatic evolution in the sense of a *digital QAA*. As a special implementation of a variational quantum algorithm (VQA) (Cerezo et al., 2021; Grange et al., 2023; Blekos et al., 2024), the key concept of QAOA is that of a *parameterized circuit*, a quantum circuit with gates that depend on real-valued parameters. Depending on the choice of parameters, executing a parameterized circuit on a QC will provide different measurement outcomes.

The goal of QAOA is to iteratively adjust the circuit parameters to guide the quantum system towards states that represent optimal or near-optimal solutions of the underlying optimization problem. This is realized along the lines of a typical QAA by starting from a problem-agnostic ground state, a balanced superposition state of every qubit, and then applying a sequence of (parameterized) gates to arrive at the problem-specific state that encodes the solution. In contrast to an analog QAA, QAOA only mimicks this transition (which may or may not yield an approximation) using a discrete sequence of gates instead of a continuous control. In the following, we describe this idea in more detail.

For a given QUBO, each qubit encodes one optimization variable. The quantum circuit is then chosen in such a way that it represents a parameterized approximation of the annealing process. The specific circuit choice is also known as *ansatz*, its *depth* is a fixed hyperparameter that denotes the number of repeating circuit elements (i.e., single gates or certain sequences of gates) in the ansatz. On the one hand, choosing a more complex ansatz (e.g., with greater depth), enables the circuit to explore more possibilities to mimic the adiabatic schedule. On the other hand, this exploration also requires to tune more parameters, which becomes computationally challenging and typically requires much more efforts to converge to a solution. These two opposing factors must be weighed against each other by the user to select a suitable ansatz (i.e., a parameterized circuit).

The role of the QPU in the hybrid QAOA setup is to run parameterized circuits and provide the measurement results, which can then be used to estimate the expectation value of the system's energy. The classical computer, on the other hand, optimizes the circuit parameters based on the QPU measurements and proposes updated parameters that aim to reduce the expected energy.

Summarized, the task of the classical computer is to effectively perform a black-box optimization under uncertainties. The objective function to be minimized is the expected energy of the quantum system and the optimization variables are the real-valued circuit parameters. In principle, this problem can be solved with any suitable classical optimization algorithm. It is a black-box optimization because the problem structure is effectively unknown. The classical optimizer can query the QPU to provide the expected energy for a given choice of circuit parameters. Gradients of the objective function can be obtained using finite differences or specialized techniques (Crooks, 2019). Uncertainties arise because of two reasons: first, the expected energy is only estimated with finite samples (each representing a QPU shot) and, second, *IBM* QCs are NISQ devices and therefore suffer from hardware-related uncertainties. Since QPU evaluations are costly, it is typically desired to find sufficiently good circuit

parameters with as few iterations (or shots) as possible. Once the optimal parameters have been found, the QPU can be used to sample solution candidates.

The device-specific workflow for the end user is summarized in Figure 3, it follows the generic quantum computing protocol from Section 3. Note that in the solution step, we do not perform a single series of shots as in the two previous approaches, but a hybrid quantum-classical optimization loop.

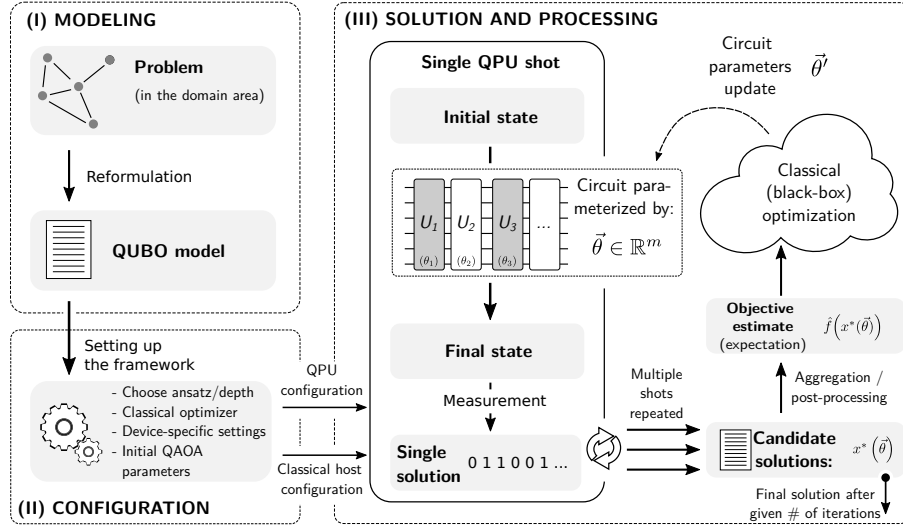


Figure 3: Workflow of the QAOA-OPT approach: solving QUBOs with a gate-based QC using QAOA.

In this paper, we only consider a foundational implementation of QAOA to illustrate the key ideas. However, from a practical perspective, fine-tuning the algorithm is an important but challenging aspect. For example, there are separate works on circuit parameter optimization (Zhou et al., 2020), initial parameter values (Sack & Serbyn, 2021; Sack et al., 2023), and the choice of classical optimizers (Cerezo et al., 2021). Improvements to the original algorithm include extensions of the aggregation function (Barkoutsos et al., 2020), counterdiabatic driving (Chandarana et al., 2022), warmstarts (Egger et al., 2021), and alternative approaches to encoding optimization constraints (Hadfield, 2018; Hadfield et al., 2019; Fuchs et al., 2022; Fuchs & Bassa, 2024), just to name a few.

In addition, there are two general technical challenges when running quantum circuits on *IBM* devices that also apply to all QPU evaluations within QAOA:

1. Limited gates: Only specific one-qubit and two-qubit gates, the so-called *basis gates*, can be executed. The set of basis gates is universal in the sense that any other gate can be decomposed into a sequence of basis gates.
2. Limited connectivity: Two-qubit gates can only be executed for specific pairs of physical qubits according to the prescribed hardware connectivity. These gaps can be bridged by the use of additional gates.

To overcome these obstacles, a classical preprocessing step called *transpilation* is necessary to transform a given quantum circuit into a hardware-compliant quantum circuit. In fact, there are infinitely many hardware-compliant quantum circuits that lead to the same measurement outcomes on an idealized (i.e., noise-free) QC. On actual *IBM* devices, however, some mathematically equivalent circuits will perform better than others. For example, as a general rule, circuits with fewer basis gates typically perform better. Moreover, each physical qubit exhibits an individual level of noise, which might also change over time (Baheri et al., 2022). Therefore, the practical performance of a quantum circuit may also depend on which physical qubits are used for its implementation. Thus, the effective goal of the transpilation is to find a hardware-compliant and well-performing representation of a given quantum circuit (Li et al., 2019; Wilson et al., 2020; Hua et al., 2023; Nation & Treinish, 2023; Waring et al., 2024).

Essentially a classical optimization problem, transpilation is solved in the *IBM* software package *Qiskit* (IBM Quantum, 2023b) with multi-step heuristics that include mapping logical qubits to physical qubits, decomposing all gates into basis gates, routing qubits with additional gates according to hardware connectivity, and an overall circuit optimization to improve the performance.

**Number of qubits needed.** In comparison with the other two approaches from Sections 3.1 and 3.2, the present approach requires fewer qubits, as summarized in Remark 1.

**Remark 1.** *An arbitrary QUBO instance with  $n$  variables that is solved with QAOA requires  $n$  quantum bits. Transpilation might affect the output quality, but it does not necessarily require additional qubits.*

## 4. Application to selected problems

In this section, we focus on three optimization problems: the traveling salesperson problem (TSP), the weighted maximum cut problem (MaxCut), and UD-MIS. We study the number of qubits it takes to solve them with the three quantum-powered optimization approaches of interest, taking into account the necessary reformulation steps. As summarized in Table 1, each of the approaches can be applied to either QUBOs or UD-MIS instances. Therefore, we start by briefly discussing these two formulations.

### 4.1. General formulation: QUBO

Assuming  $n$  binary decision variables  $x = (x_1, \dots, x_n)$ , the problem can be expressed as follows:

$$\min_x x^T Q x, \quad x \in \{0, 1\}^n, \quad (1)$$

where  $Q$  is an  $n \times n$  real-valued symmetric matrix defining the coefficients  $Q_{ij}$ . Note that the requirement to represent problems in this form is, in fact, not too restrictive. Lucas (2014) discusses so called *Ising formulations*, which are very close to QUBO, for many combinatorial optimization problems, including the 21  $\mathcal{NP}$ -hard problems from Karp's (1975) list. A tutorial by Glover et al. (2022) focuses on formulating combinatorial optimization problems as QUBOs.

Note that upper bounds on the numbers of physical qubits necessary to solve an arbitrary QUBO instance on the three selected QPUs are given by Lemmas 1 and 2 and Remark 1. These bounds are not necessarily tight and depend on properties of the matrix  $Q$ , such as sparsity. (See Appendix A.)

### 4.2. UD-MIS

Given an undirected (unit disk) graph  $G$  with node set  $V$  and edge set  $E \subseteq \binom{V}{2}$ , the maximum independent set problem seeks for a node set of the largest possible cardinality such that no two nodes in it are adjacent. Let us start with an integer programming formulation of the UD-MIS problem and then use it to formulate a corresponding QUBO instance. The problem can be modeled using one binary variable  $x_i$  for each node  $i \in V$ , indicating whether it constitutes a part of the solution, as follows.

$$\begin{aligned} \max \quad & \sum_{i \in V} x_i & (2) \\ \text{s. t.} \quad & x_i + x_j \leq 1 & \text{for all } \{i, j\} \in E, \\ & x_i \in \{0, 1\} & \text{for all } i \in V. \end{aligned}$$

To obtain an equivalent QUBO, we can introduce constraints as quadratic penalty terms corresponding to all edges  $\{i, j\} \in E$ . This results in the following formulation (expressed as a minimization

problem here, to have a uniform representation):

$$\max_{x \in \{0,1\}^{|V|}} \sum_{i \in V} x_i - M \sum_{\{i,j\} \in E} x_i x_j = - \min_{x \in \{0,1\}^{|V|}} x^T Q x, \quad \text{where } Q_{ij} = \begin{cases} -1 & \text{if } i = j, \\ M/2 & \text{if } \{i,j\} \in E, \\ 0 & \text{otherwise.} \end{cases} \quad (3)$$

Note that in the definition of  $Q_{ij}$  we consider all ordered pairs  $i, j$  to obtain a symmetric matrix. This formulation is equivalent to Equation (2) if  $M = |V| + 1$ , since in this case a single independent set constraint violation ( $x_i = x_j = 1$  for some  $\{i, j\} \in E$ ) makes this infeasible solution worse than a trivial feasible solution of  $x_1 = x_2 = \dots = x_{|V|} = 0$ . This yields the necessary number of binary variables, as stated in the following lemma.

**Lemma 3.** *For a graph  $G = (V, E)$ , the UD-MIS instance given by Equation (2) can be solved on a neutral atoms based machine with  $N := |V|$  physical qubits. The respective QUBO formulation Equation (3) requires  $N$  logical qubits. Therefore, it can be solved on a quantum annealer with Pegasus topology using at most  $24 \lceil \frac{N+10}{12} \rceil \lceil \frac{N-2}{12} \rceil$  physical qubits or on a general gate-based QC with  $N$  qubits.*

*Proof.* Follows from Lemmas 1 and 2 and Remark 1.  $\square$

### 4.3. MaxCut

Given an undirected graph  $G = (V, E)$ , the maximum cut problem seeks for a partition of the node set into two subsets, which would maximize the number of edges connecting the two subsets. This can be reformulated as an integer linear program (ILP) as follows.

$$\max \sum_{\{i,j\} \in E} e_{ij} w_{ij}, \quad (4)$$

$$\text{s. t. } e_{ij} \leq x_i + x_j \text{ for all } \{i, j\} \in E, \quad (5)$$

$$e_{ij} \leq 2 - (x_i + x_j) \text{ for all } \{i, j\} \in E, \quad (6)$$

$$x_j, e_{ij} \in \{0, 1\} \text{ for valid combinations of } i, j \in V.$$

Here,  $w_{ij} = w_{ji} \geq 0$  is the weight of the edge  $\{i, j\} \in E$ , and we assume  $i < j$  for all double-indexed variables  $e_{ij}$  corresponding to undirected edges. Variables  $x_j$  denote which set in the partition vertex  $j$  belongs to, and constraints Equation (5) and Equation (6) ensure that in an optimal solution the variable  $e_{ij} = 1$  if and only if  $\{i, j\}$  is in the cut (i.e., exactly one of  $x_i$  and  $x_j$  equals 1), and 0 otherwise.

The ILP has an elegant reformulation as a QUBO, as follows.

$$\max_{x \in \{0,1\}^n} \sum_{\{i,j\} \in E} w_{ij} (x_i + x_j - 2x_i x_j) = - \min_{x \in \{0,1\}^n} x^T Q x, \quad \text{where } Q_{ij} = \begin{cases} \sum_{k: \{i,k\} \in E} (-w_{ik}) & \text{if } i = j, \\ w_{ij} & \text{if } \{i, j\} \in E, \\ 0 & \text{otherwise.} \end{cases} \quad (7)$$

Whenever  $x_i = 1$  and  $x_j = 0$  (or vice versa), the term  $w_{ij}(x_i + x_j - 2x_i x_j)$  contributes  $w_{ij}$  to the objective. Otherwise, if  $x_i = x_j$ , the term's contribution will be zero.

**Lemma 4.** *For a graph  $G = (V, E)$ , the QUBO formulation Equation (7) of MaxCut problem requires  $N := |V|$  logical qubits. Therefore, it can be solved on a quantum annealer with Pegasus topology using at most  $24 \lceil \frac{N+10}{12} \rceil \lceil \frac{N-2}{12} \rceil$  physical qubits, on a neutral atoms QPU using  $4N^2$  physical qubits, or on a general gate-based QC with  $N$  qubits.*

*Proof.* Follows from Lemmas 1 and 2, and Remark 1.  $\square$

Note that for this problem the number of binary variables of the QUBO is only linear in the number of nodes, while for the ILP it may be quadratic, making this problem particularly suitable for QCs.

#### 4.4. TSP

Given a complete undirected graph  $G = (V, E)$  with  $N$  nodes and edge weights  $c_{ij}$ , the traveling salesperson problem (TSP) seeks for a shortest possible route in terms of the cumulative edge weight that visits each vertex exactly once and returns to the start node. On classical computers the TSP is typically solved by sophisticated ILP techniques, combined with heuristics to find a good initial solution; see [Applegate et al. \(2006\)](#). Different ILP formulations have been developed for this problem, which makes it convenient to use it as an example to compare and contrast a few alternative formulations in the context of quantum computing.

**Dantzig-Fulkerson-Johnson formulation.** The classical formulation ([Dantzig et al., 1954](#)) used in most OR textbooks implies binary variables  $x_{ij}$ ,  $i < j$ , for all edges  $\{i, j\} \in E$ , indicating that an edge is traversed by the tour:

$$\min \sum_{i < j} c_{ij} x_{ij}, \quad (\text{DFJ})$$

$$\text{s. t. } \sum_{j:j>i} x_{ij} + \sum_{j:j<i} x_{ji} = 2 \quad \text{for all } i = 1, \dots, N, \quad (8)$$

$$\sum_{\{i,j\} \in E(S)} x_{ij} \leq |S| - 1 \quad \text{for all } S \subseteq V : 3 \leq |S| \leq \frac{N}{2}, \quad (9)$$

$$x_{ij} \in \{0, 1\} \quad \text{for all } i < j,$$

where we write  $E(S) := \{\{i, j\} \mid i, j \in S, i < j\}$ , to denote a set of all edges between nodes in  $S \subseteq V$ . There are  $N$  degree constraints Equation (8), and if  $N > 5$  we also have subtour elimination constraints Equation (9). Note that Equation (9) for subsets  $S$  of size 2 is equivalent to the upper bound of the variables. In the original formulation by [Dantzig et al. \(1954\)](#) given above, we get redundant constraints if  $N$  is even, because for every set  $S$  with  $|S| = \frac{N}{2}$  we have a constraint corresponding to  $S$  and a constraint corresponding to  $V \setminus S$ . If we remove the redundant constraints, e.g., by only taking subsets of size  $\frac{N}{2}$  containing node 1, we are left with  $2^{N-1} - 1 - N - \frac{N(N-1)}{2}$  subtour elimination constraints.

In order to create an equivalent QUBO formulation, one needs to incorporate constraints into the objective function as penalty terms, involving binary variables only. Each constraint from Equation (8) induces a term of the form  $M(\sum_{j:j \neq i} x_{\{i,j\}} - 2)^2$ , but no new variables. The subtour elimination constraints, Equation (9), require slack variables in binary representation. A constraint corresponding to subset size  $|S|$  requires  $\log_2 |S| \leq \log_2 N$  new binary variables to represent the possible integer slack. Therefore, the family of constraints, Equation (9), requires at most  $(2^{N-1} - 1 - N - \frac{N(N-1)}{2}) \log_2 N$  additional binary variables. More careful calculation (presented in [Appendix B](#)) yields the following result.

**Lemma 5.** *The Dantzig-Fulkerson-Johnson ILP can be reformulated as a QUBO having*

$$n^{DFJ} := \frac{N(N-1)}{2} + \sum_{k=3}^{\lceil N/2 \rceil - 1} \binom{N}{k} \cdot \lceil \log_2(k-1) + 1 \rceil + \frac{1 + (-1)^N}{4} \cdot \binom{N}{\lfloor N/2 \rfloor} \cdot \lceil \log_2(N/2 - 1) + 1 \rceil$$

*binary variables. Therefore, it requires  $n^{DFJ}$  logical qubits and can be solved on a neutral atoms based QPU with  $4(n^{DFJ})^2$  physical qubits, a quantum annealer with  $24 \lceil \frac{n^{DFJ} + 10}{12} \rceil \lceil \frac{n^{DFJ} - 2}{12} \rceil$  physical qubits, or on a general gate-based QC with  $n^{DFJ}$  physical qubits.*

Finally, we remark that formulation Equation (DFJ) is rarely passed completely to a solver even as an integer program, but is instead used as basis for row generation approaches. It might be possible to apply a similar approach, generating penalty terms and slack variables on the fly, in an iterative quantum-classical hybrid algorithm, which might constitute an interesting research direction.

**Miller-Tucker-Zemlin formulation.** An alternative approach (Miller et al., 1960) introduces variables  $u_j \in \mathbb{N}$  denoting the number of each node  $j \in V$  in a tour. (E.g.,  $u_5 = 7$  means that node 5 is the seventh city in the tour.) We also use variables  $x_{ij}$  indicating whether edge  $\{i, j\}$  is traversed. This time, however, we also have to keep track of the traversal direction, i.e., we have two different variables  $x_{ij}$  and  $x_{ji}$  for all  $i, j \in V$  with  $i \neq j$ . Here,  $x_{ij} = 1$  indicates that  $j$  is visited directly after  $i$ . Since we assume that a tour starts at node 1, for all  $i \in V$ ,  $j \in V \setminus \{1\}$ , we must have  $u_j \geq u_i + 1$  if  $x_{ij} = 1$ . Note that such constraint would be violated by any subtour not passing through node 1. This yields:

$$\begin{aligned}
\min \quad & \sum_{i=1}^N \sum_{j:j \neq i} c_{ij} x_{ij}, & \text{(MTZ)} \\
\text{s. t.} \quad & \sum_{j:j \neq i} x_{ij} = 1 & \text{for all } i = 1, \dots, N, \\
& \sum_{i:i \neq j} x_{ij} = 1 & \text{for all } j = 1, \dots, N, \\
& u_i - u_j + (N-1)x_{ij} \leq N-2 & \text{for all } 2 \leq i, j \leq N, i \neq j, \\
& x_{ij} \in \{0, 1\} & \text{for all } 1 \leq i, j \leq N, i \neq j, \\
& u_j \geq 2 & \text{for all } j = 2, \dots, N,
\end{aligned} \tag{10}$$

where we assume the distance matrix to be symmetric:  $c_{ij} = c_{ji}$ . We have  $N(N-1)$  binary variables and  $(N-1)$  integer variables. However, now there is only a polynomial number of constraints, namely,  $2N$  degree constraints and  $(N-1)(N-2)$  constraints Equation (10) involving the new variables. In the above formulation we did not demand integrality of the  $u_j$  variables because it is not necessary and for classical hardware, omitting this constraint may accelerate the solver. In the following transformation to a QUBO, we will however assume that the  $u_j \in \mathbb{N}$ .

**Lemma 6.** *The Miller-Tucker-Zemlin integer program can be reformulated as a QUBO with*

$$n^{MTZ} := (N-1)((N-1) \cdot \lfloor \log_2(N-2) \rfloor + 2N-3)$$

*binary variables. So, it requires  $n^{MTZ}$  logical qubits and can be solved on a neutral atoms based QPU with  $4(n^{MTZ})^2$  physical qubits, a quantum annealer with  $24 \lceil \frac{n^{MTZ}+10}{12} \rceil \lceil \frac{n^{MTZ}-2}{12} \rceil$  physical qubits, or a general gate-based QC with  $n^{MTZ}$  physical qubits.*

*Proof.* The first two families of constraints give us  $2N$  penalty terms in the objective. Each integer variable  $u_j$  must be represented by binary variables. In this case we can replace  $u_j$  by  $2 + \sum_{r=0}^{\lfloor \log(N-2) \rfloor} 2^r b_{j,r}$ , introducing  $\lfloor \log(N-2) \rfloor + 1$  binary variables  $b_{j,r}$ . The slack in Equation (10) can take values from 0 (if  $j$  is the successor of  $i$ ) to  $2(N-2)$  (if  $u_i = 2, u_j = N$ ). To accommodate this range, we need  $\lfloor \log_2(N-2) \rfloor + 2$  binary variables. Since we have this for every pair of  $i, j \in \{2, \dots, N\}$  with  $i \neq j$ , the total number of such variables is  $(N-1) \cdot (N-2) \cdot (\lfloor \log_2(N-2) \rfloor + 2)$ . Therefore, the original ILP can be transformed into a QUBO model with  $2N + (N-1)(N-2)$  penalty terms, involving

$$(N-1) \cdot (\lfloor \log_2(N-2) \rfloor + 1) + (N-1) \cdot (N-2) \cdot (\lfloor \log_2(N-2) \rfloor + 2) = (N-1)((N-1)\lfloor \log_2(N-2) \rfloor + 2N-3)$$

binary variables. □

**Quadratic assignment formulation.** While these ILP approaches are very successful on classical computers, a direct translation of the formulations to QUBOs results in a large number of variables and thus of physical qubits required. In quantum computing, it makes sense to move away from ILP-based approaches and consider alternative approaches. This is well illustrated by the TSP, which actually has a very natural and compact formulation as a quadratic program, more specifically a quadratic assignment problem (see Lawler, 1963; Garfinkel, 1985, Section 4.3 on p. 27). Let us introduce binary variables  $y_{ik}$ , which equal one if and only if node  $i$  is visited during step  $k$  in the tour. Since we are interested only in tours that return to the original location, assume without loss of generality that

$y_{11} = 1$ . These ideas yield the following formulation:

$$\min \sum_{j=2}^N c_{1j} y_{j2} + \sum_{i=2}^N \left( \sum_{\substack{j=2 \\ j \neq i}}^N c_{ij} \sum_{k=2}^{N-1} y_{ik} y_{j(k+1)} + c_{1i} y_{iN} \right), \quad (\text{QAP})$$

$$\text{s. t. } \sum_{k=2}^N y_{ik} = 1 \quad \text{for all } i = 2, \dots, N. \quad (11)$$

$$\sum_{i=2}^N y_{ik} = 1 \quad \text{for all } k = 2, \dots, N. \quad (12)$$

$$y_{ik} \in \{0, 1\}, \quad \text{for all } i = 2, \dots, N \text{ and } k = 2, \dots, N$$

Each coefficient  $c_{ij}$  encodes the cost of edge  $\{i, j\} \in E$ . Whenever nodes  $i$  and  $j$  appear as consecutive steps in the tour,  $y_{ik} = y_{j(k+1)} = 1$  for some moment  $k$ , which contributes  $c_{ij}$  to the objective. The sums in the first and the last terms in Equation (QAP) implement the same logic for the first step in the tour (from node 1 to node  $j$ ), and the last one (returning from node  $i$  to node 1), respectively. Constraints Equation (11) and Equation (12) ensure that a solution represents a permutation of cities. It yields the following QUBO:

$$\min \sum_{j=2}^N c_{1j} y_{j2} + \sum_{i=2}^N \left( \sum_{\substack{j=2 \\ j \neq i}}^N c_{ij} \sum_{k=2}^{N-1} y_{ik} y_{j(k+1)} + c_{1i} y_{iN} \right) + M \sum_{i=2}^N \left( \sum_{k=2}^N y_{ik} - 1 \right)^2 + M \sum_{k=2}^N \left( \sum_{i=2}^N y_{ik} - 1 \right)^2 \quad (13)$$

$$y_{ik} \in \{0, 1\}, \quad i = 2, \dots, N \text{ and } k = 2, \dots, N$$

Formulation Equation (QAP) involved  $(N-1)^2$  binary variables,  $2(N-1)$  linear equality constraints, and a quadratic objective with  $(N-1)((N-2)^2 + 2)$  terms, which we summarize in the following result.

**Lemma 7.** *TSP over a complete graph  $G = (V, E)$  can be formulated as a QUBO with  $(N-1)^2$  binary variables. Therefore, it requires  $(N-1)^2$  logical qubits and can be solved on a neutral atoms based QPU with  $4(N-1)^4$  physical qubits, a quantum annealer with  $24 \lceil \frac{(N-1)^2 + 10}{12} \rceil \lceil \frac{(N-1)^2 - 2}{12} \rceil$  physical qubits, or a general gate-based QC with  $(N-1)^2$  physical qubits.*

Note how these three formulations yield different QUBO models, and some of them can be better in quantum computing context, although less widespread in OR literature. We summarize these differences in Table 2, where we provide the general expressions in terms of the number of nodes  $N = |V|$ , and illustrative numerical values for  $N = 10$ . For example, a naive, full Equation (DFJ) implementation would require fewest binary variables, but the exponential number of inequality constraints would yield an exponential number of variables in the QUBO model, which would translate to more than a thousand for  $N = 10$  nodes. The MTZ reformulation would reduce the number of inequality constraints and bring the number of variables in the QUBO model down to around 400. Finally, the quadratic assignment representation would not require slack variables at all, and this would result in a relatively compact QUBO model with 81 logical qubit.

## 4.5. Summary

The problems we consider in Sections 4.2 to 4.4 for the same graph size require different numbers of binary variables (that can be associated with *logical qubits*), and scale differently in terms of the number of the physical qubits. The summary of qubit requirements is presented in Table 3.

Observe that a quadratic number of QUBO variables (in terms of the number of nodes in the original graph) makes it challenging to solve TSPs on current quantum devices. In fact, given the device-dependent setup required and the best possible formulation, even 10-nodes instances will be close to the limits of the devices, and choosing a more resource-intensive formulation from Table 2

Table 2: Number of variables for TSP with  $N$  nodes: QUBO problems for different formulations.

	Dantzig-Fulkerson- Johnson Equation (DFJ)	Miller-Tucker-Zemlin Equation (MTZ)	Quadratic assignment Equation (QAP)
Constraints:			
equality	$N$	$2N$	$2(N-1)$
inequality	$2^{N-1} - 1 - \frac{N(N+1)}{2}$	$(N-1)(N-2)$	—
Variables:			
binary	$N(N-1)/2$	$N(N-1)$	$(N-1)^2$
integer	—	$N-1$	—
<b>QUBO:</b> the number of logical qubits required			
per binary	1	1	1
per integer <sup>(a)</sup>	$\leq \log_2 N$	$\leq \log_2 N$	—
total	$O(2^N \log_2 N)$	$O(N^2 \log_2 N)$	$O(N^2)$
exact formula	see Lemma 5	see Lemma 6	see Lemma 7
<b>Example:</b> a TSP on $N = 10$ nodes.			
Constraints:			
equality	10	20	18
inequality	456	72	—
Variables:			
binary	45	90	81
integer	456	9	—
<b>QUBO:</b> the number of logical qubits required			
per binary	1	1	1
per integer	$\leq 4$	$\leq 4$	—
total	$\sim 1,100$ <sup>(b)</sup>	$\sim 400$	81

<sup>a</sup> This includes slack variables (one per inequality constraint).  
based on Lemma 5.<sup>b</sup> The value of  $456 \times 4 + 45 = 1,869$  is an upper bound, but we used a refined estimate

would basically make the problem out of reach. The situation is better for MaxCut and UD-MIS instances, although, the number of required physical qubits for neutral atoms based devices for the problems that do not exhibit UD-MIS structure remains prohibitively high. At the same time, we were able to solve fairly large UD-MIS instances using the neutral atoms based device, as we will discuss further.

Overall, given the necessities of the device-dependent setup, we see QA-OPT as the most practice-ready technology of the three. QAOA-OPT represents a very interesting research direction and poses relatively modest qubit requirements, however, the method complexity and error accumulation make it harder to implement. NA-OPT also offers an interesting approach, with one of the main limitations being the necessity of the problem reformulations, along with the existing restrictions on the number of qubits available and the geometric size of the working area.

## 5. Numerical experiments

In this section, we present our results from a series of experiments aimed to illustrate the three quantum-powered optimization approaches from Section 3. An overview of the approaches is listed in Table 1. Our main goal is not to compare the performance of the state-of-the-art implementations of classical and quantum optimizers, but rather to illustrate the out-of-the-box experience with different QPUs, and to discuss the associated challenges and opportunities. Informally speaking, this is a comparison of the user experience *assuming default parameters* between the considered technologies. For this purpose, we first describe the experimental setup in Section 5.1 and subsequently report on the results in Section 5.2.



Table 3: Number of the binary variables and number of physical qubits necessary, depending on the quantum device and the problem type.

Original model		After the device-specific setup step, technology-dependent:		
Original formulation	QUBO	NA-OPT (UD-MIS representation, <a href="#">Nguyen et al., 2023</a> )	QA-OPT (clique embedding, <a href="#">Lemma 2</a> )	QAOA-OPT (no reformulation) <sup>(a)</sup>
<i>TSP over a complete graph with <math>N</math> vertices.</i> <sup>(b)</sup> <i>Quadratic assignment formulation Equation (QAP):</i>				
<ul style="list-style-type: none"> <li><math>(N - 1)^2</math> binary variables (e.g.: 81)</li> <li><math>2(N - 1)</math> equality constraints (e.g.: 18)</li> </ul>	$(N - 1)^2$ binary variables, constraints as penalties, see <a href="#">Lemma 7.</a> (e.g.: 81)	$4(N - 1)^4$ (e.g.: $\sim 26,000$ qubits)	$24 \lceil \frac{(N-1)^2+10}{12} \rceil \lceil \frac{(N-1)^2-2}{12} \rceil$ (e.g.: $\sim 1,350$ qubits)	$(N - 1)^2$ (e.g.: 81 qubits)
<i>MaxCut over a complete graph with <math>N</math> vertices,</i> <sup>(b)</sup> <i>ILP formulation Equation (4):</i>				
<ul style="list-style-type: none"> <li><math>N(N + 1)/2</math> binary variables (e.g.: 55)</li> <li><math>N(N - 1)</math> inequality constraints (e.g.: 90)</li> </ul>	$N$ binary variables, see <a href="#">Lemma 4.</a> (e.g.: 10)	$4N^2$ (e.g.: $\sim 400$ qubits)	$24 \lceil \frac{N+10}{12} \rceil \lceil \frac{N-2}{12} \rceil$ (e.g.: $\sim 50$ qubits)	$N$ (e.g.: 10 qubits)
<i>Maximum Independent Set over a graph with <math>N</math> vertices,</i> <sup>(b)</sup> <i>ILP formulation Equation (2):</i>				
<ul style="list-style-type: none"> <li><math>N</math> binary variables (e.g.: 10)</li> <li>up to <math>N(N - 1)/2</math> inequality constraints (e.g.: 45)</li> </ul>	$N$ binary variables, see <a href="#">Lemma 3.</a> (e.g.: 10)	Arbitrary graph: $4N^2$ (e.g.: $\sim 400$ qubits)  Unit disk graph: $N$ (e.g.: 10 qubits)	$24 \lceil \frac{N+10}{12} \rceil \lceil \frac{N-2}{12} \rceil$ (e.g.: $\sim 50$ qubits)	$N$ (e.g.: 10 qubits)
<i>For reference, available devices' physical qubits capacity:</i>		256	5,000+ <sup>(c)</sup>	127 and 133 <sup>(d)</sup>

<sup>a</sup> IBM gate-based QC requires device dependent *transpilation* to ensure the necessary qubit connectivity, but it usually does not require additional qubits.<sup>b</sup> Example values for  $N = 10$  are shown in parentheses.<sup>c</sup> Advantage2 machine.<sup>d</sup> As per summary on the official website at the time of writing. Systems with 433 and 1,100 qubit systems announced ([Castelvecchi, 2023](#)).

Table 4: Optimization approaches considered in our numerical experiments.

Approach	Type	Problem classes
NA-OPT	quantum-powered	UD-MIS
QA-OPT	quantum-powered	TSP, MaxCut, UD-MIS
QAOA-OPT	quantum-powered	TSP, MaxCut, UD-MIS
SIM-OPT	quantum-inspired	TSP, MaxCut, UD-MIS
Baseline	classical	TSP, MaxCut, UD-MIS

## 5.1. Setup

In the present section, we describe the setup of our numerical experiments.

**Problem instances.** For the three problem classes of interest from Section 4, we generated instances of different sizes as follows:

- TSP instances were created by randomly sampling nodes (and the corresponding distances between pairs of sampled nodes) from the TSPLIB instances (Reinelt, 1991). This allowed us to ensure the desired number of nodes in each problem while preserving the underlying graph structure corresponding to a real-world logistics network.
- MaxCut instances were created from randomly generated graphs assuming the Erdős-Rényi model (Erdős & Rényi, 1959) for different numbers of nodes and different levels of connectivity, which results in a set of QUBOs with varying sparsity.
- UD-MIS instances were specifically generated to take advantage of the physical structure of the *QuEra* device: from a randomly generated collection of points on a two-dimensional grid.

More details can be found in Appendix A.

**Optimization approaches.** We consider three kinds of optimization approaches:

- Quantum-powered approaches: These approaches, which are the primary focus of this paper, are listed in Table 1. In short, we use the NA-OPT approach to solve UD-MIS, the QA-OPT and QAOA-OPT approaches, respectively, to solve QUBO formulations of TSP, MaxCut, and UD-MIS.
- Quantum-inspired approach: In addition to the originally presented version of the QAOA-OPT approach, which runs on an *IBM* QPU, we also consider an alternative version that runs on a classical simulator instead. That is, the QPU is replaced by an idealized (i.e., noise-free) simulation of this QPU running entirely on a classical computer. We will refer to this approach as SIM-OPT in the following. It is a *quantum-inspired* approach in the sense that it relies on quantum physical laws by simulating them (to some extent), but without leveraging actual quantum physics through a QPU. The specific implementation was cloud-based 32-qubit simulator from *IBM* called *ibmq\_qasm\_simulator*.
- Baseline: As a classical baseline, we solve the respective integer programming formulations of the optimization problems with *Gurobi* (Gurobi, 2024) using default parameters. Specifically, for TSP we use the Miller-Tucker-Zemlin formulation (MTZ), for UD-MIS the natural constrained formulation (2), and for MaxCut the quadratic unconstrained formulation (7), where we set the time limit to 5 minutes per instance, or beyond that time until the optimality gap of 5% is reached, but no more than 20 minutes.

An overview is listed in Table 4.

## 5.2. Results

The evaluation of our numerical experiments is focused on two key characteristics for the end user: end-to-end algorithm runtimes and the resulting solution quality. In the following, we refer to each attempt to solve a single instance with a specific approach as a *run*. Note that for the quantum-powered approaches, a run implies aggregation over a sample of *shots* obtained from the respective QPU, which yields a single objective value (best across the sample). The runtime includes both the necessary configuration steps performed on a classical computer and the actual QPU runtime (total of all shots), but does not include the classical procedure of the problem reformulation to UD-MIS (for NA-OPT) or to QUBO (for QA-OPT and QAOA-OPT).

**Scope.** The scope of the numerical experiments is visualized in Figure 4. Each bar corresponds to the number instances of the respective type (in columns) and size (denoted along the horizontal axis) solved using the respective quantum-powered optimization approach. The three colors indicate the quality of the retrieved result, i.e., whether we were able to obtain a feasible solution (“success”), only infeasible ones (“infeasible”), or if the procedure terminated with an error or had not returned any solution for other technical reasons (“fail”). We find that the success rates vary from 100% for the NA-OPT approach, to around 75% for the QA-OPT approach, 21% for the QAOA-OPT approach, and 65% for the SIM-OPT approach. We repeated the calculations for some instances up to 4 times. Details can be found in Appendix D. (Certainly, Gurobi yielded a feasible solution every time.)

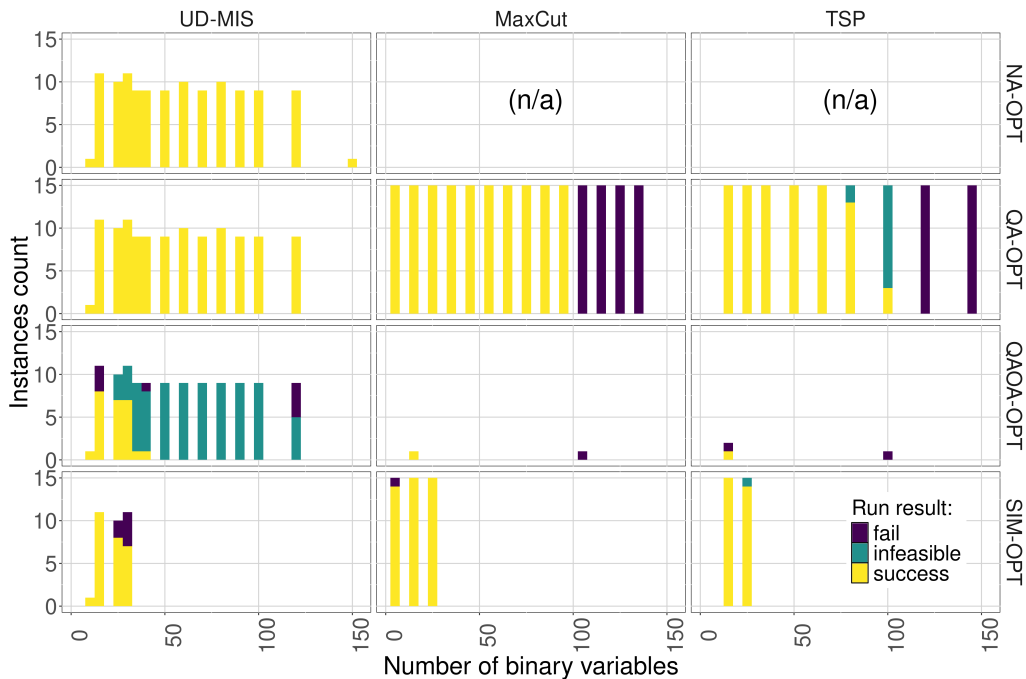


Figure 4: Number of instances across different problem sizes and types.

For the NA-OPT approach, we attempted to solve UD-MIS instances only. However, all runs were successful in the sense that we received feasible results for each one, as depicted in the first row in Figure 4. For the QA-OPT approach, we were able to successfully solve a spectrum of instances across different problem sizes and types. Note that as the problem size increases, we are starting to get more infeasible and failed experiments. A significant bottleneck here was the device-specific QPU configuration step, which is discussed further below. The QAOA-OPT approach was the least robust. We were able to solve a few small instances. Among the key practical reasons for so few instances solved are network connectivity issues and significantly longer queue waiting times for the QPU cloud service. In fact, most of the instances solved using the QAOA-OPT approach belong to the UD-MIS problem class, which is known to have more sparse QUBO matrices, see Appendix A. The lower share of successful attempts for a QPU as compared to the simulator can be also partially attributed to the convergence issues of the classical optimization loop in presence of noise. Note that

these results do not necessarily characterize the theoretical performance of variational algorithms on *IBM* hardware. However, we believe it is a good illustration of the point that QAOA-based approaches require significantly more work beyond a naive implementation in order to achieve meaningful results.

**Baseline.** The *Gurobi* approach, as the classical baseline, was able to solve all TSP instances to optimality with the largest runtime of about 15 minutes. Furthermore, the UD-MIS instances were solved to optimality in under one second. Larger MaxCut instances were more time-consuming to solve. In total, 84% of MaxCut instances were solved with optimality gap of at most 5% (more than 99% — with the gap of at most 10%). Note that there are specialized classical methods that might yield better runtimes (e.g., [Rehfeldt et al., 2023](#) for MaxCut), however, as noted above, our main goal was to compare the out-of-the-box experience, and not necessarily the state-of-the-art implementations.

**Performance metrics.** We define the relative objective deviation

$$R_f := \frac{f_q - f_c}{f_c}, \quad (14)$$

where the objective value obtained by the classical baseline is denoted by  $f_c$  and the respective value from the quantum-powered approach by  $f_q$ . Note that  $f_c$  represents the true optimal objective value only for TSP and UD-MIS instances of our dataset (as well as for *some* MaxCut instances). The last column of Table 5 represents the number of instances, where the quantum-powered approach was at least as good as the baseline, i.e., the number of cases when the respective cut value was the same *or more* as the baseline. Similarly, we define the relative deviation of the runtime

$$R_t := \frac{t_q - t_c}{t_c} \quad (15)$$

based on the runtimes of the classical baseline  $t_c$  and the quantum-powered approach  $t_q$ .

**Runtimes.** For the comparably small problem instances we considered, the runtimes for quantum-powered workflows were mostly above the ones for the classical baseline, as presented in Figure 5. Each point represents a single run, and the tilted line in the top left corner reflects the situation when the runtimes are equal to the baseline. Note that there is a sub-collection of problems that took the Gurobi solver more time to solve than our QPU-based heuristic, which constitutes the set of points above the tilted line. It entirely consists of larger MaxCut instances, and investigating the structure of these problems in the context of possible application areas of quantum computing to OR might constitute an interesting further research direction.

**Objective values.** The relative deviations of the objective values, Equation (14), are summarized in Table 5. The last column represents the number of instances, where the quantum-powered approach was at least as good as the baseline, i.e., the number of cases when the respective cut value was the same *or more* as the baseline.

For both MaxCut and TSP the quantum-powered approaches often provided solutions within 25% of the optimal value. Interestingly, for the subset of “hard” MaxCut instances, where the classical solver took more than 20 seconds to solve (depicted in the right panel of Figure 5), the QA-OPT approach was often able to find a solution within 10–15% from the baseline, in only half of the respective runtime. Note that we obtained the quantum-powered results for such large instances only with the QA-OPT approach.

Solution quality in terms of the relative objective values for UD-MIS instances turned out to be somewhat lower than for other problem classes. This is surprising, given that QUBO matrices for these problems were significantly less dense as compared to, for example, MaxCut problems. There might be several reasons for this effect. Note that relative objective deviations are sensitive to costs associated with single bit-flips. In other words, a change in a single bit in the solution might yield different objective adjustments, depending on the combination of the problem type and the costs. Further, for the NA-OPT approach, a geometric arrangement of the atoms for accurate problem representation

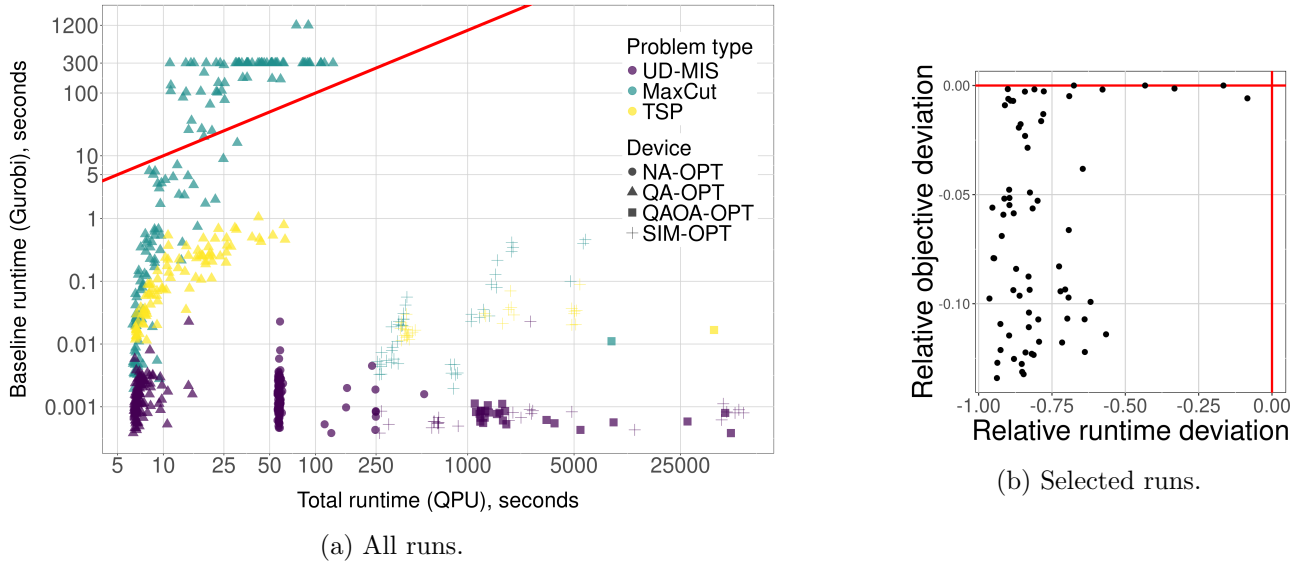


Figure 5: Relative runtime and objective value deviations from the baseline, as defined in Equations (14) and (15).

Table 5: Summary of the deviations between the objective values: QPU-based vs. baseline.

Problem type	Device	No. of instance runs with relative objective deviations:								
		Total	within 25%	within 10%	within 5%	no worse (0%)				
UD-MIS	NA-OPT	117	93	79.5%	48	41.0%	34	29.1%	30	25.6%
	QA-OPT	116	116	100%	77	66.4%	54	46.6%	46	39.7%
	QAOA-OPT	25	9	36.0%	2	8.0%	2	8.0%	2	8.0%
	SIM-OPT	27	8	29.6%	3	11.1%	3	11.1%	3	11.1%
MaxCut	QA-OPT	149	149	100%	128	85.9%	105	70.5%	50	33.6%
	QAOA-OPT	1	1	100%	0	0%	0	0%	0	0%
	SIM-OPT	44	44	100%	44	100%	44	100%	20	45.5%
TSP	QA-OPT	91	61	67.0%	49	53.8%	46	50.5%	37	40.7%
	QAOA-OPT	1	1	100%	1	100%	0	0%	0	0%
	SIM-OPT	29	26	89.7%	22	75.9%	20	69.0%	17	58.6%

might pose additional challenges. Finally, the structure of constraints might play a role. At the same time, we must emphasize that the number of instances (especially for the QAOA-OPT approach) is too low to make any statistically significant conclusions. We believe that investigating these effects in detail is outside the scope of our paper, however, describing which problem characteristics make it difficult or easy for different quantum-powered methods constitute an interesting further research direction. The dataset of problems presented here could provide a good starting point for such analysis. A few selected examples of solutions from the quantum-powered approaches are presented in Appendix F.

**Minor embeddings.** To conclude, we report two key aspects of the necessary embedding process within the QA-OPT approach. First, the runtime of a classical computer to find the embedding and, second, the number of physical qubits necessary to realize it (which can be more than number of optimization variables of the underlying QUBO due to the introduction of chains). We found that the bounds on the necessary numbers of qubits presented in Lemma 2 and Table 3 were not always tight. The heuristic algorithm used to find embeddings in practice (Cai et al., 2014) performed better than the upper bound given in Lemma 2. Further, due to differences in problem structure, namely the QUBO matrix sparsity (see Appendix A), the dependence between the number of logical and physical qubits was different for different types of problems. For the problem with  $n$  binary variables, using

ordinary least squares regression in logarithmic scale, we estimate the required number of physical qubits to constitute around  $O(n^{1.8})$  for MaxCut and TSP instances, and around  $O(n^{1.1})$  for UD-MIS. See Appendix E for details. With the aim to study characteristics of instances that could benefit from a QC, Gilbert et al. (2024) performed experiments on crafted instances of  $\mathcal{NP}$ -hard problems whose QUBO graph is a subgraph of the topology graph, so that it can be embedded without overhead.

The embedding process also entails significant (classical) runtime costs. In our case, it dominated the solution time for large enough TSP and MaxCut instances, as illustrated in Figure 6. For more sparse UD-MIS instances with comparable numbers of binary variables, finding embeddings was relatively easy. While the embedding time varied with the number of binary variables in general, we did not scale the allotted annealing time. Therefore, for large and dense instances, up to 90% of the total runtime was spent trying to find an embedding, before starting the actual computation on the QPU.

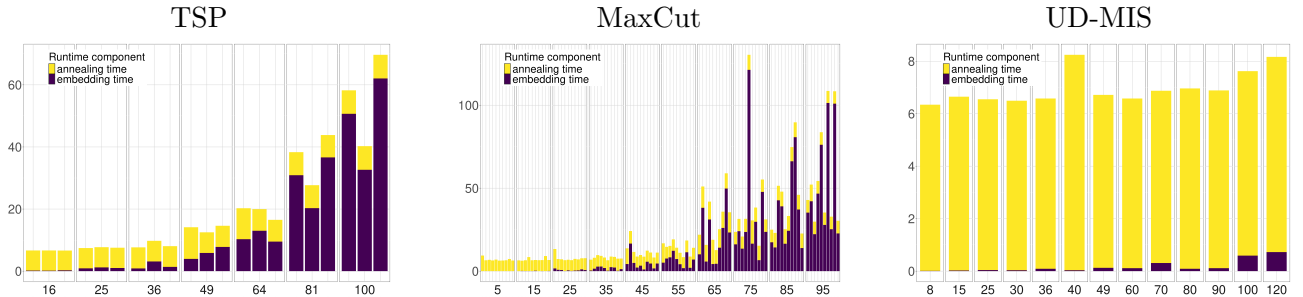


Figure 6: Efforts to compute minor embeddings for the QA-OPT approach. Shown is the embedding time (on a classical computer; dark color) vs. annealing time (QPU; light color), in seconds; different scales for different problem types on vertical axis. Each bar represents runtime for an instance of the given size (number of QUBO variables, horizontal axis; randomly selected instances for each problem size).

## 6. Conclusion

In general, it is difficult to assess which of the currently available systems is superior. Different quantum algorithms might have different requirements for the hardware, and device properties might affect the details of the algorithm implementations. As a result, the development of hardware and the development of algorithms for practical applications goes together. This is why we did not try to benchmark methods, but highlighted three specific quantum-powered approaches to solve discrete optimization problems. As listed in Table 1, we considered two analog approaches, NA-OPT (solving UD-MIS with an analog QC based on neutral atom technology) and QA-OPT (solving QUBOs with a quantum annealer based on superconducting technology), as well as a digital approach, QAOA-OPT (solving QUBOs with a gate-based QC based on superconducting technology). The paper offers three groups of key contributions.

First, we provide a high-level overview of the relevant workflows, aiming at a general OR audience. To the best of our knowledge, this is the first attempt to describe several different quantum approaches in a uniform framework as sketched in Figure 1. We hope this effort will help motivate further involvement of the OR community into quantum optimization research. Fine-tuning of quantum algorithms and careful modeling of optimization problems may allow alternative quantum-powered solution strategies and therefore pose novel research opportunities (Blekos et al., 2024).

Second, we show that the required number of qubits for an optimization problem is not just a characteristic of the problem itself, but can be dramatically affected by the chosen quantum technology, problem type, and the specific formulation, as listed in Tables 2 and 3.

Third, we highlight a few crucial practical issues. Note how the device-specific setup gives rise to an auxiliary classical optimization problems, which is typically solved on a classical computer and might constitute a source for interdisciplinary collaborations between the quantum computing and OR communities. We discuss the embedding process within the QA-OPT approach in the context of the required additional runtime and requirements for the number of qubits. We did not analyze the

similar transpilation step within the QAOA-OPT approach, although, quantitative assessment of the effects of this step on the solutions quality might constitute an interesting further research direction. Also, improving heuristic approaches that yield reasonable device configurations might increase the practicality of all of the three quantum-powered approaches considered in this paper.

The quality of the obtained numerical solutions depends on the problem type, but in general our classical baseline (solving an integer programming model using a state of the art commercial solver) outperformed the quantum-powered approaches, given enough time. However, even with all the restrictions of the available quantum devices, we were able to generate a collection of MaxCut instances that were hard enough for the classical solver, and for which we were able to obtain heuristic solutions from the quantum device with reasonable quality faster than using a classical solver. Our experiments highlight the obvious fact that QUBO matrix sparsity affects the problem complexity, both for the classical and quantum-powered approaches. However, characterizing classes of difficult (or easy) problems for QCs constitute another direction of the fundamental research.

## References

- Abbas, A., Ambainis, A., Augustino, B., Bärttschi, A., Buhrman, H., Coffrin, C., Cortiana, G., Dunjko, V., Egger, D.J., Elmegreen, B.G., Franco, N., Fratini, F., Fuller, B., Gacon, J., Gonciulea, C., Gribling, S., Gupta, S., Hadfield, S., Heese, R., Kircher, G., Kleinert, T., Koch, T., Korpas, G., Lenk, S., Marecek, J., Markov, V., Mazzola, G., Mensa, S., Mohseni, N., Nannicini, G., O'Meara, C., Tapia, E.P., Pokutta, S., Proissl, M., Rebstrost, P., Sahin, E., Symons, B.C.B., Tornow, S., Valls, V., Woerner, S., Wolf-Bauwens, M.L., Yard, J., Yarkoni, S., Zechiel, D., Zhuk, S., Zoufal, C., 2023. Quantum optimization: Potential, challenges, and the path forward. Preprint. doi:[10.48550/arxiv.2312.02279](https://doi.org/10.48550/arxiv.2312.02279).
- Albash, T., Lidar, D.A., 2018. Adiabatic quantum computation. *Reviews of Modern Physics* 90, 015002. doi:[10.1103/revmodphys.90.015002](https://doi.org/10.1103/revmodphys.90.015002), [arXiv:1611.04471](https://arxiv.org/abs/1611.04471).
- Amazon Web Services, 2020. Amazon Braket. URL: <https://aws.amazon.com/braket/>.
- Applegate, D.L., Bixby, R.E., Chvátal, V., Cook, W.J., 2006. The Traveling Salesman Problem: A Computational Study. volume 17 of *Princeton Series in Applied Mathematics*. Princeton University Press, Princeton. doi:[10.1515/9781400841103](https://doi.org/10.1515/9781400841103).
- Au-Yeung, R., Chancellor, N., Halffmann, P., 2023. NP-hard but no longer hard to solve? Using quantum computing to tackle optimization problems. *Frontiers in Quantum Science and Technology* 2, 1128576. doi:[10.3389/frqst.2023.1128576](https://doi.org/10.3389/frqst.2023.1128576), [arXiv:2212.10990](https://arxiv.org/abs/2212.10990).
- Baheri, B., Guan, Q., Chaudhary, V., Li, A., 2022. Quantum noise in the flow of time: A temporal study of the noise in quantum computers, in: *IEEE 28th International Symposium on On-Line Testing and Robust System Design (IOLTS)*, pp. 1–5. doi:[10.1109/IOLTS56730.2022.9897404](https://doi.org/10.1109/IOLTS56730.2022.9897404).
- Barkoutsos, P.K., Nannicini, G., Robert, A., Tavernelli, I., Woerner, S., 2020. Improving variational quantum optimization using CVaR. *Quantum* 4, 256. doi:[10.22331/q-2020-04-20-256](https://doi.org/10.22331/q-2020-04-20-256), [arXiv:1907.04769](https://arxiv.org/abs/1907.04769).
- Bera, M.N., Acín, A., Kuś, M., Mitchell, M.W., Lewenstein, M., 2017. Randomness in quantum mechanics: philosophy, physics and technology. *Reports on Progress in Physics* 80, 124001. doi:[10.1088/1361-6633/aa8731](https://doi.org/10.1088/1361-6633/aa8731), [arXiv:1611.02176](https://arxiv.org/abs/1611.02176).
- Blekos, K., Brand, D., Ceschini, A., Chou, C.H., Li, R.H., Pandya, K., Summer, A., 2024. A review on quantum approximate optimization algorithm and its variants. *Physics Reports* 1068, 1–66. doi:[10.1016/j.physrep.2024.03.002](https://doi.org/10.1016/j.physrep.2024.03.002), [arXiv:2306.09198](https://arxiv.org/abs/2306.09198).
- Bolusani, S., Besançon, M., Bestuzheva, K., Chmiela, A., Dionísio, J., Donkiewicz, T., van Doornmalen, J., Eifler, L., Ghannam, M., Gleixner, A., Graczyk, C., Halbig, K., Hedtke, I., Hoen, A., Hojny, C., van der Hulst, R., Kamp, D., Koch, T., Kofler, K., Lentz, J., Manns, J., Mexi, G., Mühmer, E., Pfetsch, M.E., Schlösser, F., Serrano, F., Shinano, Y., Turner, M., Vigerske, S., Weninger, D., Xu, L., 2024. The SCIP optimization suite 9.0. Preprint. doi:[10.48550/arXiv.2402.17702](https://doi.org/10.48550/arXiv.2402.17702).

- Boothby, K., Bunyk, P., Raymond, J., Roy, A., 2020. Next-generation topology of D-Wave quantum processors. Preprint. doi:[10.48550/arXiv.2003.00133](https://doi.org/10.48550/arXiv.2003.00133).
- Boothby, T., King, A.D., Roy, A., 2016. Fast clique minor generation in Chimera qubit connectivity graphs. *Quantum Information Processing* 15, 495–508. doi:[10.1007/s11128-015-1150-6](https://doi.org/10.1007/s11128-015-1150-6), [arXiv:1507.04774](https://arxiv.org/abs/1507.04774).
- Cai, J., Macready, W.G., Roy, A., 2014. A practical heuristic for finding graph minors. Preprint. doi:[10.48550/arXiv.1406.2741](https://doi.org/10.48550/arXiv.1406.2741).
- Castelvecchi, D., 2023. IBM releases first-ever 1,000-qubit quantum chip. *Nature* 624, 238. doi:[10.1038/d41586-023-03854-1](https://doi.org/10.1038/d41586-023-03854-1).
- Cerezo, M., Arrasmith, A., Babbush, R., Benjamin, S.C., Endo, S., Fujii, K., McClean, J.R., Mitarai, K., Yuan, X., Cincio, L., Coles, P.J., 2021. Variational quantum algorithms. *Nature Reviews Physics* 3, 625–644. doi:[10.1038/s42254-021-00348-9](https://doi.org/10.1038/s42254-021-00348-9), [arXiv:2012.09265](https://arxiv.org/abs/2012.09265).
- Chandarana, P., Hegade, N.N., Paul, K., Albarrán-Arriagada, F., Solano, E., del Campo, A., Chen, X., 2022. Digitized-counterdiabatic quantum approximate optimization algorithm. *Physical Review Research* 4. doi:[10.1103/physrevresearch.4.013141](https://doi.org/10.1103/physrevresearch.4.013141), [arXiv:2107.02789](https://arxiv.org/abs/2107.02789).
- Choi, V., 2008. Minor-embedding in adiabatic quantum computation: I. The parameter setting problem. *Quantum Information Processing* 7, 193–209. doi:[10.1007/s11128-008-0082-9](https://doi.org/10.1007/s11128-008-0082-9), [arXiv:0804.4884](https://arxiv.org/abs/0804.4884).
- Choi, V., 2011. Minor-embedding in adiabatic quantum computation: II. Minor-universal graph design. *Quantum Information Processing* 10, 343–353. doi:[10.1007/s11128-010-0200-3](https://doi.org/10.1007/s11128-010-0200-3), [arXiv:1001.3116](https://arxiv.org/abs/1001.3116).
- Clark, B.N., Colbourn, C.J., Johnson, D.S., 1990. Unit disk graphs. *Discrete Mathematics* 86, 165–177. doi:[10.1016/0012-365X\(90\)90358-0](https://doi.org/10.1016/0012-365X(90)90358-0).
- Crooks, G.E., 2019. Gradients of parameterized quantum gates using the parameter-shift rule and gate decomposition. Preprint. doi:[10.48550/arXiv.1905.13311](https://doi.org/10.48550/arXiv.1905.13311).
- D-Wave, 2024. D-Wave Leap. URL: <https://cloud.dwavesys.com>.
- D-Wave, n.d. D-Wave QPU Architecture: Topologies. D-Wave Systems Inc. URL: [https://docs.dwavesys.com/docs/latest/c\\_gs\\_4.html](https://docs.dwavesys.com/docs/latest/c_gs_4.html). accessed online 2024-07-22.
- Dantzig, G., Fulkerson, R., Johnson, S., 1954. Solution of a large-scale traveling-salesman problem. *Journal of the Operations Research Society of America* 2, 393–410. doi:[10.1287/opre.2.4.393](https://doi.org/10.1287/opre.2.4.393).
- Date, P., Patton, R., Schuman, C., Potok, T., 2019. Efficiently embedding QUBO problems on adiabatic quantum computers. *Quantum Information Processing* 18, 117. doi:[10.1007/s11128-019-2236-3](https://doi.org/10.1007/s11128-019-2236-3).
- Dattani, N., Szalay, S., Chancellor, N., 2019. Pegasus: The second connectivity graph for large-scale quantum annealing hardware. Preprint. doi:[10.48550/arxiv.1901.07636](https://doi.org/10.48550/arxiv.1901.07636).
- Ebadi, S., Keesling, A., Cain, M., Wang, T.T., Levine, H., Bluvstein, D., Semeghini, G., Omran, A., Liu, J., Samajdar, R., Luo, X.Z., Nash, B., Gao, X., Barak, B., Farhi, E., Sachdev, S., Gemelke, N., Zhou, L., Choi, S., Pichler, H., Wang, S., Greiner, M., Vuletić, V., Lukin, M.D., 2022. Quantum optimization of maximum independent set using Rydberg atom arrays. *Science* 376, 1209–1215. doi:[10.1126/science.abo6587](https://doi.org/10.1126/science.abo6587), [arXiv:2202.09372](https://arxiv.org/abs/2202.09372).
- Ebadi, S., Wang, T.T., Levine, H., Keesling, A., Semeghini, G., Omran, A., Bluvstein, D., Samajdar, R., Pichler, H., Ho, W.W., Choi, S., Sachdev, S., Greiner, M., Vuletić, V., Lukin, M.D., 2021. Quantum phases of matter on a 256-atom programmable quantum simulator. *Nature* 595, 227–232. doi:[10.1038/s41586-021-03582-4](https://doi.org/10.1038/s41586-021-03582-4), [arXiv:2012.12281](https://arxiv.org/abs/2012.12281).
- Egger, D.J., Mareček, J., Woerner, S., 2021. Warm-starting quantum optimization. *Quantum* 5, 479. doi:[10.22331/q-2021-06-17-479](https://doi.org/10.22331/q-2021-06-17-479), [arXiv:2009.10095](https://arxiv.org/abs/2009.10095).
- Erdős, P., Rényi, A., 1959. On random graphs I. *Publicationes Mathematicae Debrecen* 6, 290–297. doi:[10.5486/pmd.1959.6.3-4.12](https://doi.org/10.5486/pmd.1959.6.3-4.12).



- Farhi, E., Goldstone, J., Gutmann, S., 2014. A quantum approximate optimization algorithm. Preprint. doi:[10.48550/arXiv.1411.4028](https://doi.org/10.48550/arXiv.1411.4028).
- Farhi, E., Goldstone, J., Gutmann, S., Sipser, M., 2000. Quantum computation by adiabatic evolution. Preprint. doi:[10.48550/arXiv.quant-ph/0001106](https://doi.org/10.48550/arXiv.quant-ph/0001106).
- Fuchs, F.G., Bassa, R.P., 2024. Optimal mixers restricted to subspaces and the stabilizer formalism. Preprint. doi:[10.48550/arXiv.2306.17083](https://doi.org/10.48550/arXiv.2306.17083).
- Fuchs, F.G., Lye, K.O., Møll Nilsen, H., Stasik, A.J., Sartor, G., 2022. Constraint preserving mixers for the quantum approximate optimization algorithm. *Algorithms* 15, 202. doi:[10.3390/a15060202](https://doi.org/10.3390/a15060202), [arXiv:2203.06095](https://arxiv.org/abs/2203.06095).
- Garfinkel, R.S., 1985. Motivation and modeling, in: Lawler, E.L., Lenstra, J.K., Rinnooy Kan, A.H.G., Shmoys, D.B. (Eds.), *The Traveling Salesman Problem*. Wiley, Chichester, UK. Wiley Series in Discrete Mathematics & Optimization. chapter 2, pp. 17–36.
- Gilbert, V., Rodriguez, J., Louise, S., 2024. Benchmarking quantum annealers with near-optimal minor-embedded instances. Preprint. doi:[10.48550/arXiv.2405.01378](https://doi.org/10.48550/arXiv.2405.01378).
- Glover, F., Kochenberger, G., Hennig, R., Du, Y., 2022. Quantum bridge analytics I: a tutorial on formulating and using QUBO models. *Annals of Operations Research* 314, 141–183. doi:[10.1007/s10479-022-04634-2](https://doi.org/10.1007/s10479-022-04634-2).
- Goswami, K., Mukherjee, R., Ott, H., Schmelcher, P., 2024. Solving optimization problems with local light shift encoding on Rydberg quantum annealers. *Physical Review Research* 6, 023031. doi:[10.1103/physrevresearch.6.023031](https://doi.org/10.1103/physrevresearch.6.023031), [arXiv:2308.07798](https://arxiv.org/abs/2308.07798).
- Grange, C., Poss, M., Bourreau, E., 2023. An introduction to variational quantum algorithms for combinatorial optimization problems. *4OR* 21, 363–403. doi:[10.1007/s10288-023-00549-1](https://doi.org/10.1007/s10288-023-00549-1), [arXiv:2212.11734](https://arxiv.org/abs/2212.11734).
- Gurobi, 2024. Gurobi Optimizer Reference Manual. Gurobi Optimization, LLC. URL: <https://www.gurobi.com>.
- Gyongyosi, L., Imre, S., 2019. A survey on quantum computing technology. *Computer Science Review* 31, 51–71. doi:[10.1016/j.cosrev.2018.11.002](https://doi.org/10.1016/j.cosrev.2018.11.002).
- Hadfield, S., Wang, Z., O’Gorman, B., Rieffel, E.G., Venturelli, D., Biswas, R., 2019. From the quantum approximate optimization algorithm to a quantum alternating operator ansatz. *Algorithms* 12, 34. doi:[10.3390/a12020034](https://doi.org/10.3390/a12020034), [arXiv:1709.03489](https://arxiv.org/abs/1709.03489).
- Hadfield, S.A., 2018. *Quantum Algorithms for Scientific Computing and Approximate Optimization*. Ph.D. thesis. Columbia University. doi:[10.7916/D8X650C9](https://doi.org/10.7916/D8X650C9), [arXiv:1805.03265](https://arxiv.org/abs/1805.03265).
- Harrow, A.W., Montanaro, A., 2017. Quantum computational supremacy. *Nature* 549, 203–209. doi:[10.1038/nature23458](https://doi.org/10.1038/nature23458), [arXiv:1809.07442](https://arxiv.org/abs/1809.07442).
- Hoeffler, T., Häner, T., Troyer, M., 2023. Disentangling hype from practicality: On realistically achieving quantum advantage. *Communications of the ACM* 66, 82–87. doi:[10.1145/3571725](https://doi.org/10.1145/3571725), [arXiv:2307.00523](https://arxiv.org/abs/2307.00523).
- Hua, F., Wang, M., Li, G., Peng, B., Liu, C., Zheng, M., Stein, S., Ding, Y., Zhang, E.Z., Humble, T., Li, A., 2023. QASMTrans: A QASM quantum transpiler framework for NISQ devices, in: *Proceedings of the SC ’23 Workshops of The International Conference on High Performance Computing, Network, Storage, and Analysis*, ACM, New York, NY, USA. p. 1468–1477. doi:[10.1145/3624062.3624222](https://doi.org/10.1145/3624062.3624222), [arXiv:2308.07581](https://arxiv.org/abs/2308.07581).
- IBM Quantum, 2023a. URL: <https://quantum.ibm.com/>.
- IBM Quantum, 2023b. IBM Quantum Documentation: Transpiler. IBM. URL: <https://docs.quantum.ibm.com/api/qiskit/transpiler>.
- Karp, R.M., 1975. On the computational complexity of combinatorial problems. *Networks* 5, 45–68. doi:[10.1002/net.1975.5.1.45](https://doi.org/10.1002/net.1975.5.1.45).

- Klug, F., 2024. Quantum optimization algorithms in operations research: methods, applications, and implications. Preprint. doi:[10.48550/arXiv.2312.13636](https://doi.org/10.48550/arXiv.2312.13636).
- Klymko, C., Sullivan, B.D., Humble, T.S., 2013. Adiabatic quantum programming: minor embedding with hard faults. *Quantum Information Processing* 13, 709–729. doi:[10.1007/s11128-013-0683-9](https://doi.org/10.1007/s11128-013-0683-9), [arXiv:1210.8395](https://arxiv.org/abs/1210.8395).
- Lawler, E.L., 1963. The quadratic assignment problem. *Management Science* 9, 586–599. URL: <https://www.jstor.org/stable/2627364>, doi:[10.1287/mnsc.9.4.586](https://doi.org/10.1287/mnsc.9.4.586).
- Li, G., Ding, Y., Xie, Y., 2019. Tackling the qubit mapping problem for NISQ-era quantum devices, in: *Proceedings of the Twenty-Fourth International Conference on Architectural Support for Programming Languages and Operating Systems*, ACM. pp. 1001–1014. doi:[10.1145/3297858.3304023](https://doi.org/10.1145/3297858.3304023), [arXiv:1809.02573](https://arxiv.org/abs/1809.02573).
- Lobe, E., Lutz, A., 2024. Minor embedding in broken chimera and derived graphs is NP-complete. *Theoretical Computer Science* 989, 114369. doi:[10.1016/j.tcs.2023.114369](https://doi.org/10.1016/j.tcs.2023.114369), [arXiv:2110.08325](https://arxiv.org/abs/2110.08325).
- Lobe, E., Schürmann, L., Stollenwerk, T., 2021. Embedding of complete graphs in broken Chimera graphs. *Quantum Information Processing* 20, 234. doi:[10.1007/s11128-021-03168-z](https://doi.org/10.1007/s11128-021-03168-z), [arXiv:2012.12720](https://arxiv.org/abs/2012.12720).
- Lubinski, T., Coffrin, C., McGeoch, C., Sathe, P., Apanavicius, J., Bernal Neira, D., 2024. Optimization applications as quantum performance benchmarks. *ACM Transactions on Quantum Computing* doi:[10.1145/3678184](https://doi.org/10.1145/3678184), [arXiv:2302.02278](https://arxiv.org/abs/2302.02278).
- Lucas, A., 2014. Ising formulations of many NP problems. *Frontiers in Physics* 2, 5. doi:[10.3389/fphy.2014.00005](https://doi.org/10.3389/fphy.2014.00005), [arXiv:1302.5843](https://arxiv.org/abs/1302.5843).
- Markidis, S., 2024. What is quantum parallelism, anyhow? Preprint. doi:[10.48550/arXiv.2405.07222](https://doi.org/10.48550/arXiv.2405.07222).
- McGeoch, C., Farré, P., 2020. The D-Wave Advantage System: An Overview. Technical Report 14-1049A-A. D-Wave Systems Inc. URL: <https://www.dwavesys.com/resources/white-paper/the-d-wave-advantage-system-an-overview/>.
- Miller, C.E., Tucker, A.W., Zemlin, R.A., 1960. Integer programming formulation of traveling salesman problems. *Journal of the ACM* 7, 326–329. doi:[10.1145/321043.321046](https://doi.org/10.1145/321043.321046).
- Mücke, S., Gerlach, T., Piatkowski, N., 2023. Optimum-preserving QUBO parameter compression. Preprint. doi:[10.48550/arXiv.2307.02195](https://doi.org/10.48550/arXiv.2307.02195).
- Nation, P.D., Treinish, M., 2023. Suppressing quantum circuit errors due to system variability. *PRX Quantum* 4, 010327. doi:[10.1103/PRXQuantum.4.010327](https://doi.org/10.1103/PRXQuantum.4.010327), [arXiv:2209.15512](https://arxiv.org/abs/2209.15512).
- Nguyen, M.T., Liu, J.G., Wurtz, J., Lukin, M.D., Wang, S.T., Pichler, H., 2023. Quantum optimization with arbitrary connectivity using Rydberg atom arrays. *PRX Quantum* 4, 010316. doi:[10.1103/PRXQuantum.4.010316](https://doi.org/10.1103/PRXQuantum.4.010316), [arXiv:2209.03965](https://arxiv.org/abs/2209.03965).
- Nielsen, M.A., Chuang, I.L., 2010. *Quantum Computation and Quantum Information*. 10th anniversary ed., Cambridge University Press, Cambridge, New York. doi:[10.1017/CB09780511976667](https://doi.org/10.1017/CB09780511976667).
- Parekh, O., 2023. Synergies between operations research and quantum information science. *INFORMS Journal on Computing* 35, 266–273. doi:[10.1287/ijoc.2023.1268](https://doi.org/10.1287/ijoc.2023.1268), [arXiv:2301.05554](https://arxiv.org/abs/2301.05554).
- Pelofske, E., 2023. Comparing three generations of D-Wave quantum annealers for minor embedded combinatorial optimization problems. Preprint. doi:[10.48550/arXiv.2301.03009](https://doi.org/10.48550/arXiv.2301.03009).
- Pelofske, E., 2024. 4-clique network minor embedding for quantum annealers. *Physical Review Applied* 21, 034023. doi:[10.1103/PhysRevApplied.21.034023](https://doi.org/10.1103/PhysRevApplied.21.034023), [arXiv:2301.08807](https://arxiv.org/abs/2301.08807).
- Pelofske, E., Hahn, G., Djidjev, H., 2020. Advanced unembedding techniques for quantum annealers, in: *2020 International Conference on Rebooting Computing (ICRC)*, IEEE. pp. 34–41. doi:[10.1109/ICRC2020.2020.00001](https://doi.org/10.1109/ICRC2020.2020.00001), [arXiv:2009.05028](https://arxiv.org/abs/2009.05028).
- Pichler, H., Wang, S.T., Zhou, L., Choi, S., Lukin, M.D., 2018. Quantum optimization for maximum independent set using Rydberg atom arrays. Preprint. doi:[10.48550/arxiv.1808.10816](https://doi.org/10.48550/arxiv.1808.10816).

- Preskill, J., 2018. Quantum computing in the NISQ era and beyond. *Quantum* 2, 79. doi:[10.22331/q-2018-08-06-79](https://doi.org/10.22331/q-2018-08-06-79), [arXiv:1801.00862](https://arxiv.org/abs/1801.00862).
- Rehfeldt, D., Koch, T., Shinano, Y., 2023. Faster exact solution of sparse MaxCut and QUBO problems. *Mathematical Programming Computation* 15, 445–470. doi:[10.1007/s12532-023-00236-6](https://doi.org/10.1007/s12532-023-00236-6).
- Reinelt, G., 1991. TSPLIB—a traveling salesman problem library. *ORSA Journal on Computing* 3, 376–384. doi:[10.1287/ijoc.3.4.376](https://doi.org/10.1287/ijoc.3.4.376).
- Sack, S.H., Medina, R.A., Kueng, R., Serbyn, M., 2023. Recursive greedy initialization of the quantum approximate optimization algorithm with guaranteed improvement. *Physical Review A* 107, 062404. doi:[10.1103/PhysRevA.107.062404](https://doi.org/10.1103/PhysRevA.107.062404), [arXiv:2209.01159](https://arxiv.org/abs/2209.01159).
- Sack, S.H., Serbyn, M., 2021. Quantum annealing initialization of the quantum approximate optimization algorithm. *Quantum* 5, 491. doi:[10.22331/q-2021-07-01-491](https://doi.org/10.22331/q-2021-07-01-491), [arXiv:2101.05742](https://arxiv.org/abs/2101.05742).
- Scholten, T.L., Williams, C.J., Moody, D., Mosca, M., Hurley, W., Zeng, W.J., Troyer, M., Gambetta, J.M., 2024. Assessing the benefits and risks of quantum computers. Preprint. doi:[10.48550/arXiv.2401.16317](https://doi.org/10.48550/arXiv.2401.16317).
- Serret, M.F., Marchand, B., Ayril, T., 2020. Solving optimization problems with Rydberg analog quantum computers: Realistic requirements for quantum advantage using noisy simulation and classical benchmarks. *Physical Review A* 102, 052617. doi:[10.1103/PhysRevA.102.052617](https://doi.org/10.1103/PhysRevA.102.052617), [arXiv:2006.11190](https://arxiv.org/abs/2006.11190).
- Shor, P.W., 1997. Polynomial-time algorithms for prime factorization and discrete logarithms on a quantum computer. *SIAM Journal on Computing* 26, 1484–1509. doi:[10.1137/S0097539795293172](https://doi.org/10.1137/S0097539795293172).
- Venegas-Andraca, S.E., Cruz-Santos, W., McGeoch, C., Lanzagorta, M., 2018. A cross-disciplinary introduction to quantum annealing-based algorithms. *Contemporary Physics* 59, 174–197. doi:[10.1080/00107514.2018.1450720](https://doi.org/10.1080/00107514.2018.1450720), [arXiv:1803.03372](https://arxiv.org/abs/1803.03372).
- Waring, J.B., Pere, C., Beux, S.L., 2024. Noise aware utility optimization of NISQ devices. Preprint. doi:[10.48550/arXiv.2402.08226](https://doi.org/10.48550/arXiv.2402.08226).
- Wilson, E., Singh, S., Mueller, F., 2020. Just-in-time quantum circuit transpilation reduces noise, in: 2020 IEEE International Conference on Quantum Computing and Engineering (QCE), IEEE. pp. 345–355. doi:[10.1109/QCE49297.2020.00050](https://doi.org/10.1109/QCE49297.2020.00050), [arXiv:2005.12820](https://arxiv.org/abs/2005.12820).
- Wintersperger, K., Dommert, F., Ehmer, T., Hoursanov, A., Klepsch, J., Mauerer, W., Reuber, G., Strohm, T., Yin, M., Lubner, S., 2023. Neutral atom quantum computing hardware: Performance and end-user perspective. *EPJ Quantum Technology* 10, 32. doi:[10.1140/epjqt/s40507-023-00190-1](https://doi.org/10.1140/epjqt/s40507-023-00190-1), [arXiv:2304.14360](https://arxiv.org/abs/2304.14360).
- Wurtz, J., Bylinskii, A., Braverman, B., Amato-Grill, J., Cantu, S.H., Huber, F., Lukin, A., Liu, F., Weinberg, P., Long, J., Wang, S.T., Gemelke, N., Keesling, A., 2023. Aquila: QuEra’s 256-qubit neutral-atom quantum computer. Preprint. doi:[10.48550/arXiv.2306.11727](https://doi.org/10.48550/arXiv.2306.11727).
- Wurtz, J., Lopes, P.L.S., Gorgulla, C., Gemelke, N., Keesling, A., Wang, S., 2022. Industry applications of neutral-atom quantum computing solving independent set problems. Preprint. doi:[10.48550/arxiv.2205.08500](https://doi.org/10.48550/arxiv.2205.08500).
- Zbinden, S., Bärtschi, A., Djidjev, H., Eidenbenz, S., 2020. Embedding algorithms for quantum annealers with Chimera and Pegasus connection topologies, in: Sadayappan, P., Chamberlain, B.L., Juckeland, G., Ltaief, H. (Eds.), *High Performance Computing*, Springer International Publishing, Cham. pp. 187–206. doi:[10.1007/978-3-030-50743-5\\_10](https://doi.org/10.1007/978-3-030-50743-5_10).
- Zhou, L., Wang, S.T., Choi, S., Pichler, H., Lukin, M.D., 2020. Quantum approximate optimization algorithm: Performance, mechanism, and implementation on near-term devices. *Physical Review X* 10, 021067. doi:[10.1103/PhysRevX.10.021067](https://doi.org/10.1103/PhysRevX.10.021067), [arXiv:1812.014041](https://arxiv.org/abs/1812.014041).

## Appendix A Instance generation

We use randomized procedures to generate our collection of problem instances, which comprises three problem types. For each type, we create problems of varying sizes (see Figure 4 for a summary) and problem structures, as presented below.

**Traveling Salesperson problem.** In order to preserve the structure of the underlying graphs, resembling real-world transportation networks, we sampled nodes from existing traveling salesperson problem (TSP) instances (Reinelt, 1991). In particular, we picked 15 instances at random from TSPLIB, and sampled the desired number of nodes from each one randomly, preserving edge weights. Therefore, each original TSPLIB instance yielded a collection of TSP problems constituting complete graphs of the given sizes, with the same distances structure as compared to the original instance.

**Weighted Maximum Cut problem.** The collection of instances was created by generating a set of random graphs  $G(N, p)$  of different sizes using the Erdős-Rényi random graph model (Erdős & Rényi, 1959). Namely, first  $N$  nodes are created, and then each pair is connected by an edge at random, independently, with the given probability  $p$ . Across the studied problem sizes, we generate graphs for the values of  $p = 0.25, 0.5,$  and  $0.75$ . Costs are generated uniformly at random, within given limits. This procedure results in graphs of different connectivity depending on the parameter  $p$ . Three characteristic examples of such graphs are presented in Figure 7.

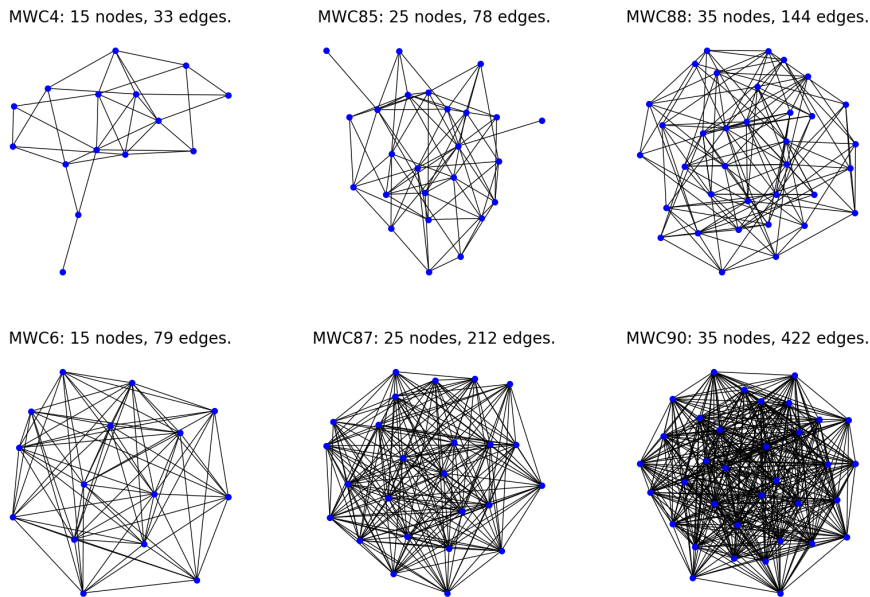


Figure 7: Sample weighted maximum cut problem (MaxCut) instances. The graphs in the left column correspond to  $p = 0.25$ , in the middle column to  $p = 0.5$ , and in the right column to  $p = 0.75$ .

**Unit Disk Maximum Independent Set problem.** The instances are generated from sets of points in a way to ensure compatibility with the neutral atoms based machine. First, we fix the coordinate window, specifying the maximum integer values for each point coordinate,  $W$  and  $H$ . Then we create a grid of points with all possible integer coordinates  $(x, y)$  for  $0 \leq x \leq W$  and  $0 \leq y \leq H$ . Finally, the points are deleted one by one at random, until the desired total number of points is reached. An instance is specified by such a set of points and a real parameter  $R$ , the *blockade radius*, implying that there is an edge between any two points whose Euclidean distance is no more than  $R$ . Variations in the coordinate window size allow us to generate instances of different points density on the coordinate plane, leading to different graph connectivity. (Three characteristic examples of such instances are presented in Figure 8.) Namely, for each studied problem size  $N$ , we fix the window to  $W_N \times H_N := (\lceil \sqrt{N} \rceil + 1) \times (\lceil \sqrt{N} \rceil + 1)$  to generate a set of points. We use three different values of  $R$  to

create different connectivity patterns in the grid of points, and repeat the procedure to generate three instances for each set of parameters. Further, we created 9 instances with hand-picked parameters for manual inspection: with a fixed value of  $R = 1.5$ , three different window sizes, and varying number of nodes between 8 and 150.

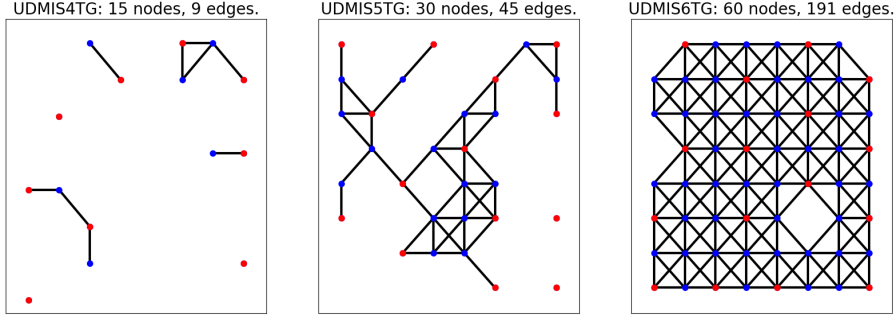


Figure 8: Sample maximum independent set problem on a unit disk graph (UD-MIS) instances. Same radius parameter and window size, varying numbers of nodes. (Close enough nodes are connected with an edge.)

This approach allows us to consider different structures of the problems with respect to the resulting quadratic unconstrained binary optimization problem (QUBO) matrices, as depicted in Figure 9. Namely, MaxCut problems allow us to vary the density of QUBO matrix in our dataset. The three values of the node connectivity parameter (0.25, 0.5, and 0.75) used in instance generation correspond to the three groups of MaxCut instances (dark circles) in the figure. For large enough instances these values approximately equal the shares of nonzero entries in the matrix. Our UD-MIS instances (light squares) imply significantly less dense QUBO matrices, mostly due to the node degree restriction, related to the hardware limitations. TSP instances (triangles) occupy the middle position in terms of the matrix sparsity.

Let us provide a brief theoretical illustration for the share of nonzero entries in the QUBO matrix for different types of problems.

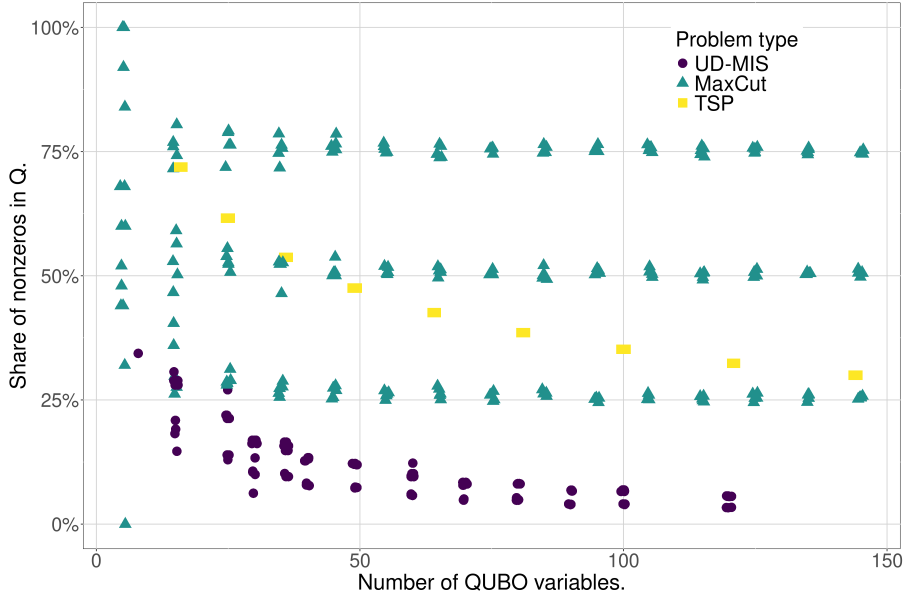


Figure 9: Share of nonzero entries in QUBO matrix for different types of problems. Three bands of points for MaxCut instances in the figure correspond to different parameter values  $p = 0.25$ , 0.5, and 0.75 (bottom to top).

**UD-MIS.** The QUBO matrix  $Q$  defined by Equation (3) has  $2|E| + |V|$  nonzero entries. If the node degree is bounded from above by some value  $d$  that is independent of  $N$  (as it is the case in our experiments), the total number of nonzero entries in  $Q$  is at most  $2N(d/2) + N = N(d + 1)$ . Since the total number of entries in  $Q$  is  $N^2$ , the share of nonzero entries is  $N(d + 1)/N^2 = (d + 1)/N$ , decreasing as the problem scales up.

**MaxCut.** The number of nonzero entries in matrix  $Q$  given by Equation (7) is  $2|E| + |V|$ . Note that we deliberately generate instances with different node connectivity by varying node connectivity parameter  $p$  in Erdős-Rényi model, taking values of 0.25, 0.5, and 0.75. If the number of edges is  $qN(N - 1)/2 \in O(N^2)$  for some real number  $q$  between zero and one, the share of nonzero entries in  $Q$  will constitute:

$$\frac{2qN(N - 1)/2 + N}{N^2} = q + (1 - q)/N \in O(1),$$

as the problem scales up with fixed  $q$ . Namely, the share of nonzero entries in  $Q$  will approach the parameter  $p$  used during the instance generation, as the number of nodes  $N$  grows. (Note that the MaxCut instances clearly split into three groups in Figure 9, corresponding to different values of parameter  $p$ .)

**TSP.** The number of nonzero entries in the matrix  $Q$  defined by Equation (13) is in  $O(N^3)$ , out of  $(N - 1)^4$  entries in  $Q$  in total, and hence the share of nonzero entries belongs to  $O(1/N)$ .

## Appendix B Required number of logical qubits for QUBO formulation of the TSP

We will derive the result of Lemma 5 stating the necessary number of logical qubits for the QUBO reformulation of the TSP integer program Equation (DFJ). This formulation involves binary variables only, but we still need to introduce penalty terms in order to transform it to an equivalent QUBO. The equality constraints can be directly translated to quadratic penalty terms: For each  $i \in V$ , the constraint  $\sum_{j:j>i} x_{ij} + \sum_{j:j<i} x_{ji} = 2$  induces the term  $M(\sum_{j:j>i} x_{ij} + \sum_{j:j<i} x_{ji} - 2)^2$  in the QUBO objective function, where  $M$  must be sufficiently large (e.g.,  $M = N^2 \max_{\{i,j\} \in E} c_{ij}$ ) to separate feasible and infeasible solutions in terms of the objective values. Inequality constraints Equation (9) have to be converted to equalities by introducing integer slack variables. So, we replace every inequality constraint of the form

$$\sum_{\{i,j\} \in E(S)} x_{ij} \leq |S| - 1$$

with the corresponding pair of constraints

$$\sum_{\{i,j\} \in E(S)} x_{ij} + s_S = |S| - 1, \quad s_S \geq 0.$$

This transformation introduces new integer variables  $s_S$ , and we further substitute them with their binary representations. For every subset  $S$  with  $3 \leq |S| \leq \frac{N}{2}$  the sum  $\sum_{\{i,j\} \in E(S)} x_{ij}$  can take values between 0 (if no two nodes from  $S$  are visited consecutively) and  $|S| - 1$  (if all nodes from  $Q$  are visited consecutively). Therefore, we need binary variables  $b_{S,r}$  for  $r = 0, \dots, \lfloor \log_2(|S| - 1) \rfloor$ , so that we replace  $s_S$  by  $\sum_{r=0}^{\lfloor \log_2(|S| - 1) \rfloor} 2^r b_{S,r}$ , which can take all values between 0 and  $|S| - 1$ . After this replacement, we can again derive quadratic penalty terms of the form

$$M \cdot \left( \sum_{\{i,j\} \in E(S)} x_{ij} + \sum_{r=0}^{\lfloor \log_2(|S| - 1) \rfloor} 2^r b_{S,r} - (|S| - 1) \right)^2$$

for  $M$  large enough.

Therefore, for a DFJ model we will have a corresponding QUBO with  $\frac{N(N-1)}{2} + O(2^N \log N)$  binary variables and  $2^{N-1} - \frac{N(N-1)}{2} - 1$  penalty terms in the objective. To calculate the number of slack variables more precisely, note that we have  $\binom{N}{3}$  constraints with slack at most two,  $\binom{N}{4}$  constraints with slack at most three, and so on. The resulting number of slack variables is then

$$\begin{aligned} & \sum_{k=3}^{(N-1)/2} \binom{N}{k} \cdot \lfloor \log_2(k-1) + 1 \rfloor && \text{if } N \text{ is odd,} \\ & \sum_{k=3}^{N/2-1} \binom{N}{k} \cdot \lfloor \log_2(k-1) + 1 \rfloor + \frac{1}{2} \binom{N}{N/2} \cdot \lfloor \log_2(N/2-1) + 1 \rfloor && \text{if } N \text{ is even.} \end{aligned}$$

Therefore, we arrive at the desired result: When applying the standard procedure to reformulate the Dantzig-Fulkerson-Johnson integer linear program (ILP), Equation (DFJ), as a QUBO, the result has

$$\frac{N(N-1)}{2} + \sum_{k=3}^{\lceil N/2 \rceil - 1} \binom{N}{k} \cdot \lfloor \log_2(k-1) + 1 \rfloor + \frac{1 + (-1)^N}{4} \cdot \binom{N}{\lfloor N/2 \rfloor} \cdot \lfloor \log_2(N/2-1) + 1 \rfloor$$

binary variables. The first summand here gives the number of binary variables in the ILP. The next two summands give the number of new binary variables to represent the possible slacks. They generalize the two terms given above for odd or even  $N$  and are derived by summing over all considered subset sizes and taking the number of such subsets times the necessary number of binary variables to represent the possible slack.

## Appendix C Computational workflows summary

Details for the three key steps of the computational workflow mentioned in Figure 1 are summarized in Table 6. First, the discrete optimization problem at hand must be reformulated: our approach involving the neutral atoms device admits UD-MIS problems only, while quantum annealing and quantum approximate optimization algorithm (QAOA) allow for arbitrary QUBO models. Then, the quantum processing unit (QPU) and classical host machine (defining the computational framework) need to be configured. The quantum device configuration is usually prepared in a device-independent way, and then translated into the language of device-specific instructions. Different technologies require different amounts of computational overhead for this step. For the machines from *IBM* and *QuEra*, device configuration is relatively straightforward, while the *D-Wave* quantum annealer requires the solution of an additional optimization problem of graph embedding to start the computation. Finally, the solution step is different across the three technologies. The neutral atoms based machine and the quantum annealer function in a similar (analog) mode, where the initial state is prepared, then a pre-defined evolution schedule is executed, and the result is read out. This process is repeated multiple times to obtain a distribution of solutions and try to alleviate the possible errors due to hardware limitations. QAOA is a variational algorithm, and its computation stage is different as it comprises a classical outer black box optimization loop. However, after the solution is found, the processing is usually similar: the quantum state corresponding to the best found ansatz parameters is constructed and measured multiple times to obtain a sample of solutions to the original problem.

Table 6: Key high-level steps of the computational workflow.

Step	NA-OPT	QA-OPT	QAOA-OPT	
0) Formulation	The problem is reformulated as UD-MIS <sup>a</sup>		A QUBO <sup>b</sup> model.	
1) QPU setup	Describing the initial state and key parameters of the quantum device:			
CONFIGURATION	1.1) Device-independent configuration	Prepare problem-dependent spatial configuration for the atoms (the atoms array) and define the blockade radius.	Set up annealing time.	Design the quantum circuit (ansatz): <ul style="list-style-type: none"> <li>• build the operators <math>U_M</math> and <math>U_P</math>,</li> <li>• choose circuit depth.</li> </ul>
	1.2) Device-dependent configuration	Translate the setup to physical device commands (automatically).	Embedding: map logical qubits to the device nodes: <ul style="list-style-type: none"> <li>• choose required “chain strength”,</li> <li>• find the mapping.</li> </ul>	The circuit is “transpiled” for the specific device: <ul style="list-style-type: none"> <li>• map the gates to device-native gates,</li> <li>• add SWAP gates to ensure necessary qubit connectivity.</li> </ul>
	2) Framework parameters.	<ul style="list-style-type: none"> <li>• Set up Hamiltonian evolution schedule.</li> <li>• Choose the number of shots.</li> </ul>	<ul style="list-style-type: none"> <li>• Choose the number of shots (sample size),</li> <li>• implement the objective calculation procedure.</li> </ul>	<ul style="list-style-type: none"> <li>• Choose initial circuit parameters,</li> <li>• implement objective function estimation,</li> <li>• set up a classical solver to find parameters.</li> </ul>
SOLUTION / PROCESSING	3) Computation	Candidate solutions are sampled from the multiple shots of the QPU. During each step: <ul style="list-style-type: none"> <li>• prepare and initialize the device,</li> <li>• realize the evolution schedule,</li> <li>• sample a (single) solution.</li> </ul>	Candidate solutions are sampled from the multiple shots of the QPU, each one comprising the following steps: <ul style="list-style-type: none"> <li>• prepare and initialize the device,</li> <li>• anneal (converges the state to a low-energy one),</li> <li>• sample a (single) solution.</li> </ul>	<ul style="list-style-type: none"> <li>• Given the circuit parameters, the QPU is set up to output a candidate solution.</li> <li>• An auxiliary objective is set up as a function that takes circuit parameters, samples candidate solutions from QPU, and returns the QUBO objective.</li> <li>• A classical black-box optimizer searches for circuit parameter values that minimize the auxiliary objective, iteratively querying the QPU.</li> <li>• A set of solutions is sampled from multiple shots of QPU, given the best circuit parameters found.</li> </ul>
	4) Post-processing	Recover MIS solution(s): e.g., the most frequently sampled one.	Recover QUBO solution(s): broken chains resolved (e.g., majority vote) → QUBO solution for each shot.	Recover QUBO solution(s), analyze convergence data.

<sup>a</sup> S-weighted version of the problem and the respective maximum-weight independent set problem on unit disk graph (UD-MWIS) reformulation (Nguyen et al., 2023) if node-specific detuning is allowed by the hardware.

<sup>b</sup> The software might be able to reformulate some other representations to QUBO automatically, e.g., incorporating constraints, integer variables, etc.



## Appendix D Summary of the different runs across instances.

Calculations for some of the instances were repeated several times, to possibly obtain a feasible solution, or for technical reasons related to the interactions with the remote machines. Summary of all attempts is presented in Figure 10. Each bar corresponds to a single instance, and counts correspond to the number of times the respective instance of the given type (in columns) was solved by each QPU (in rows). Colors mark the run results: whether we were able to retrieve a feasible solution, only infeasible ones, or no solutions at all. The instances are sorted by size, in the number of QUBO variables, which is summarized into three groups (no more than 25 variables, between 26 and 100, and more than 100 variables) for readability.

For our analysis in the main text of the paper, we selected one run per instance (which is summarized in Figure 4), as follows. If we were able to obtain a feasible solution, we used the latest run that yielded one. Otherwise, we used the latest run among those that yielded at least an infeasible solution, or just the latest run if all of them failed.



Figure 10: Summary of the different QPU runs across problem instances.

## Appendix E Qubit cost of embedding: regressions summary

This section focuses on the costs of embeddings in terms of additional qubits necessary for computation on the *D-Wave*'s quantum annealing.

Consider a model equivalent to the power law for the number of physical qubits  $Q_e$  used after embedding as a function of the number of qubits in the original QUBO model:

$$\log Q_e = \log \text{Const} + \beta \log Q_{\text{QUBO}} + \varepsilon,$$

where the error term, denoted  $\varepsilon$ , captures the discrepancies with the experimental data. Since the share of nonzero entries in the QUBO matrix scales differently (Figure 9), it seems reasonable to expect that the number of physical qubits would scale differently with the problem size, as a function of the number of logical qubits. This translates to the different slopes of the fitted lines in Figure 11. Each point in the figure represents a solved instance (random horizontal jitter added for visibility), with the color indicating the problem type. Dashed lines of the respective colors represent fitted ordinary least square regressions in logarithms. Axes' tick marks are in the natural logarithm scale. Note that for the same number of logical qubits, UD-MIS requires noticeably fewer physical qubits as compared to MaxCut and TSP.

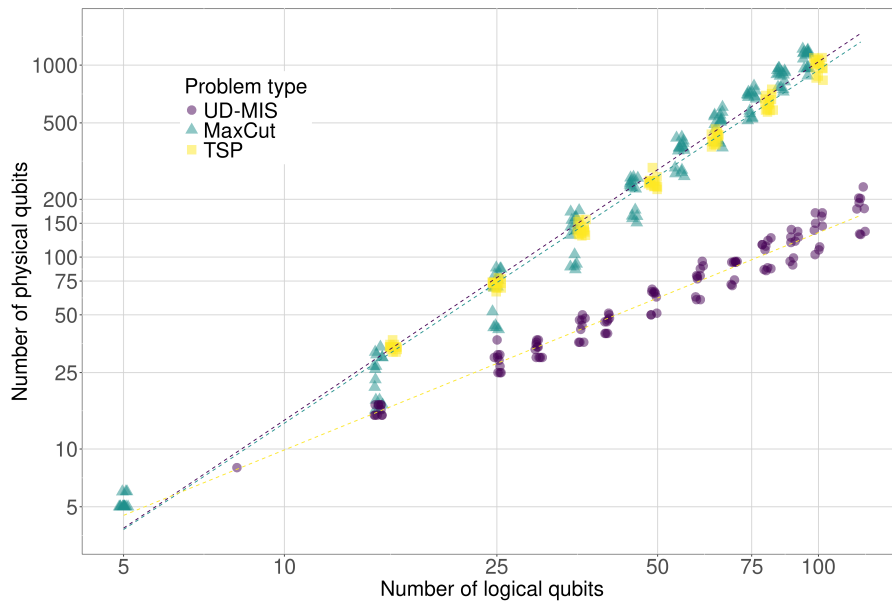


Figure 11: The number of physical vs. logical qubits, logarithmic scale.

The regressions summaries are presented in Table 7

## Appendix F Sample outputs from QPUs

Usually, a QPU output constitutes a sample of solutions obtained from a series of shots. (The number of shots is a parameter chosen at the configuration step. We tried to pick a large enough number, while maintaining reasonable total runtimes.) Figures 12, 13, and 15 present such samples for three selected runs, for each of the three technologies.

For example, Figure 12 summarizes three samples for the *D-Wave* QPU in our experiment. Each bar represents a single solution, “solution count” denotes the number of times this solution was sampled, and “energy” reflects the objective representation for the solution within the QPU (which is an actual energy of the physical system in the corresponding state). “QUBO objective” presents an objective value calculated from a QUBO formulation, and “original objective” corresponds to the objective for the original problem. (Note that for feasible solutions the latter two might differ only in sign, and no original objective values correspond to infeasible solutions.) Thick horizontal line in the bottom panel represents the optimal objective value. The panel entitled “ch. breaks” represents the share of chain

Table 7: Physical vs. logical qubits for *D-Wave* embeddings: fitted regression lines.

	<i>Dependent variable:</i>		
	log( $Q_e$ ), in different regressions:		
	UD-MIS	MaxCut	TSP
$\beta$ : log( $Q_{\text{QUBO}}$ )	1.132*** (0.020)	1.867*** (0.023)	1.840*** (0.012)
$\beta_0 = \log \text{Const}$	-0.316*** (0.080)	-1.652*** (0.085)	-1.626*** (0.044)
Observations	116	150	105
R <sup>2</sup>	0.964	0.978	0.996
Adjusted R <sup>2</sup>	0.964	0.978	0.996
Residual Std. Error	0.139 (df = 114)	0.243 (df = 148)	0.072 (df = 103)
F Statistic	3,064.768*** (df = 1; 114)	6,679.321*** (df = 1; 148)	25,468.300*** (df = 1; 103)

*Note:* standard errors are in parentheses, *df* denotes degrees of freedom \*\*\*  $p < 0.01$

breaks—a measure of the quality of the measured solution. (Note how chain breaks appear only for the largest instance in the figure.)

We see varying quality of the representation for the true objective with the quantum state. The top panel of Figure 12 shows a typical “favorable case:” all the solutions are feasible (there are no feasibility constraints for MaxCut), and most of the sampled solutions are optimal or close to optimal. The middle panel, highlighting a five-nodes TSP instance with internal ID TSP53 (having  $(N - 1)^2 = 16$  binary variables in the QUBO), depicts a more mixed picture. Most of the sampled solutions were feasible (although not all), and the algorithm was able to find a true optimum. However, it was not the most frequently sampled solution. The bottom panel presents an even more pessimistic case of a larger TSP with ID TSP82 and 49 QUBO variables, an 8-node TSP instance. First of all, most of the sampled solutions were actually infeasible for the original problem (hence, representing significantly suboptimal solutions to the corresponding QUBO). The solution frequency profile is not very pronounced, without clear maxima and most of the solutions sampled once or twice. The quality of the solution is worse, and there is a strictly positive absolute gap between the best found solution and a true optimum.

A similar situation is illustrated in Figure 13 for the *QuEra*’s device. Again, the top panel represents a relatively favorable situation where more than half of the solutions are feasible, and the most frequently sampled one corresponds to a true optimum. In the middle panel, a significant number of solutions were sampled one or two times, but the frequency profile still has a maximum around a true optimal solution. The bottom panel represents yet another instance (which is approximately four times as large as the one corresponding to the top panel), and here we see a completely flat frequency profile of the sample: each solution was sampled exactly once. Such a difference in output quality is somewhat surprising, as the three instances mentioned here are very close in terms of the structure (see Figure 14), and in fact represent different numbers of similar, but unrelated UD-MIS problems, which are solved in parallel within a single shot. This highlights the fact that quantum-powered algorithms are complex and sometimes might require additional fine-tuning. Some “best practices” and practical considerations aiming specifically at the *Aquila* device are discussed by [Wurtz et al. \(2023\)](#).

Outputs for the same three instances from *IBM*’s devices is presented in Figure 15. For these instance sizes, the simulator was able to find more feasible solutions, but overall the picture is the same. The smallest instance, UDMIS1TG, yields a reasonable solution frequency profile. Approximately doubling the number of variables results in most of the solutions being sampled once or twice, and doubling the number of variables again yields a completely flat frequency profile (1000 different solu-

tions sampled, out of 1000 attempts), with noticeable number of infeasible solutions (more so for an actual quantum device as compared to the simulator). Finally, it is interesting to note that the *QuEra* device, while offering less flexibility than the general gate-based device from *IBM*, does seem to yield better solutions for UD-MIS instances, with our naive implementation.

## Appendix G D-Wave embeddings: Chimera and Pegasus topology graphs

For the *D-Wave* annealers, the qubits are realized as superconducting loops, which can be represented as horizontal or vertical segments, and a coupler between two qubits exists only when the segments intersect. Hence, the topology graphs of these QPUs are intersection graphs of axis-parallel segments. An example, the so-called *Chimera* topology, is shown in Figure 16: the top left panel shows the intersecting segments (thick lines), where intersections of two neighboring horizontal or vertical qubits are represented by thin lines between them. The resulting topology graph  $G_T$  is shown in the top right panel.

One safe way to obtain an embedding of the QUBO graph  $G_Q$  into  $G_T$  is to search for an embedding of a clique  $K_n$  into  $G_T$ , which allows to realize all possible interactions. The problem of finding the largest clique minor in a broken topology graph is fixed-parameter tractable in the number of broken qubits (Lobe et al., 2021), i.e., it can be solved exactly with running time polynomial in the size of the topology graph (but exponential in the number of broken qubits). In this paper, for our upper bounds on the number of physical qubits required, we consider clique embeddings into the non-broken Pegasus graph, described below. In practice, broken qubits may turn these embeddings invalid and lead to a larger number of qubits, but on the other hand, the graphs  $G_Q$  resulting from our application problems are usually rather sparse, which allows for a significant reduction of qubits required as compared to our bound, which is confirmed by our experimental results, see Section 5.2.

To explain the clique embedding, let us first consider the Chimera topology, shown in Figure 16, which was used by a previous generation of *D-Wave* QPUs. It consists of eight-qubit cells, tiled vertically and horizontally, and connected to each other as presented in the top right panel of Figure 16. Each cell constitutes a complete bipartite graph with four nodes on each side, denoted as  $K_{4,4}$ . The nodes from one of the bipartition classes (“horizontal qubits”, corresponding to horizontal segments) are connected to their counterparts in the horizontally neighboring cells, while the nodes from the other bipartition class (“vertical qubits”) are connected to the vertically neighboring cells. Every node has degree at most 6, which makes it in particular necessary to use multiple nodes (i.e., physical qubits) to represent a variable interacting with more than six other variables. Choi (2011) described a variant of clique embedding where always four chains are grouped together and each  $K_{4,4}$  realizes the interactions within one such group or between two such groups (see also Klymko et al., 2013; Boothby et al., 2016; Date et al., 2019). For example, in Figure 16, a quadruple of binary variables  $x_1, \dots, x_4$  is involved in five cells, one for the interactions within the quadruple and one for the interactions with each other variable quadruple. Distinct quadruples are denoted by distinct colors in the figure; the high-level logic is presented in the bottom panel.

The topology graph of the Advantage device, the so called *Pegasus* graph (Boothby et al., 2020; Dattani et al., 2019; D-Wave, n.d.), consists of three Chimera graphs with additional connections, see Figure 17. Each inner node has, besides the six incident edges from its Chimera graph, one additional incident edge to a neighbored node from its cell (breaking the bipartiteness) and eight edges to nodes from the other two Chimera graphs, which results in a total node degree of 15. The connections between different Chimera graphs within the Pegasus graph are designed in a way that combining the Chimera embeddings of three cliques  $K_n$  yields an embedding of  $K_{3n}$  (with some caution at the boundaries). This means that in order to embed a clique of  $12n$  logical qubits, we can subdivide this into three cliques of size  $4n$  and embed each into a Chimera consisting of  $n^2$   $K_{4,4}$ -cells, resulting in  $3n^2$  cells, while an embedding into a single Chimera graph would require  $(3n)^2$  cells. Hence, (ignoring boundary effects), the number of required physical qubits to embed a clique into the new graph is divided by three. Therefore, for either of the two topology graphs, an arbitrary QUBO with  $n$  variables can be encoded using  $O(n^2)$  physical qubits, although with different hidden constants. Pelofske (2023)

provides a detailed comparison of *D-Wave*'s device topologies. The exact number for Pegasus is given in the following lemma.

**Lemma 8** (Boothby et al., 2020). *For every  $M \in \mathbb{N}$  the clique  $K_{12M-10}$  is a minor of a Pegasus graph consisting of  $24M(M-1)$  nodes corresponding to physical qubits.*

This result immediately gives us that if we want to embed  $n$  logical qubits, then we can apply the lemma to  $M = \lceil \frac{n+10}{12} \rceil \leq \frac{n+21}{12}$ , resulting in at most  $\frac{(n+9)(n+21)}{6}$  physical qubits for an connected QUBO instance, as presented in Lemma 2

Another representation of the experimental data with respect to annealing time and embedding time separately is given in Figure 18. The left panel presents annealing time in seconds (without the embedding), while embedding time shares across all the instances in our dataset are summarized in the right panel.

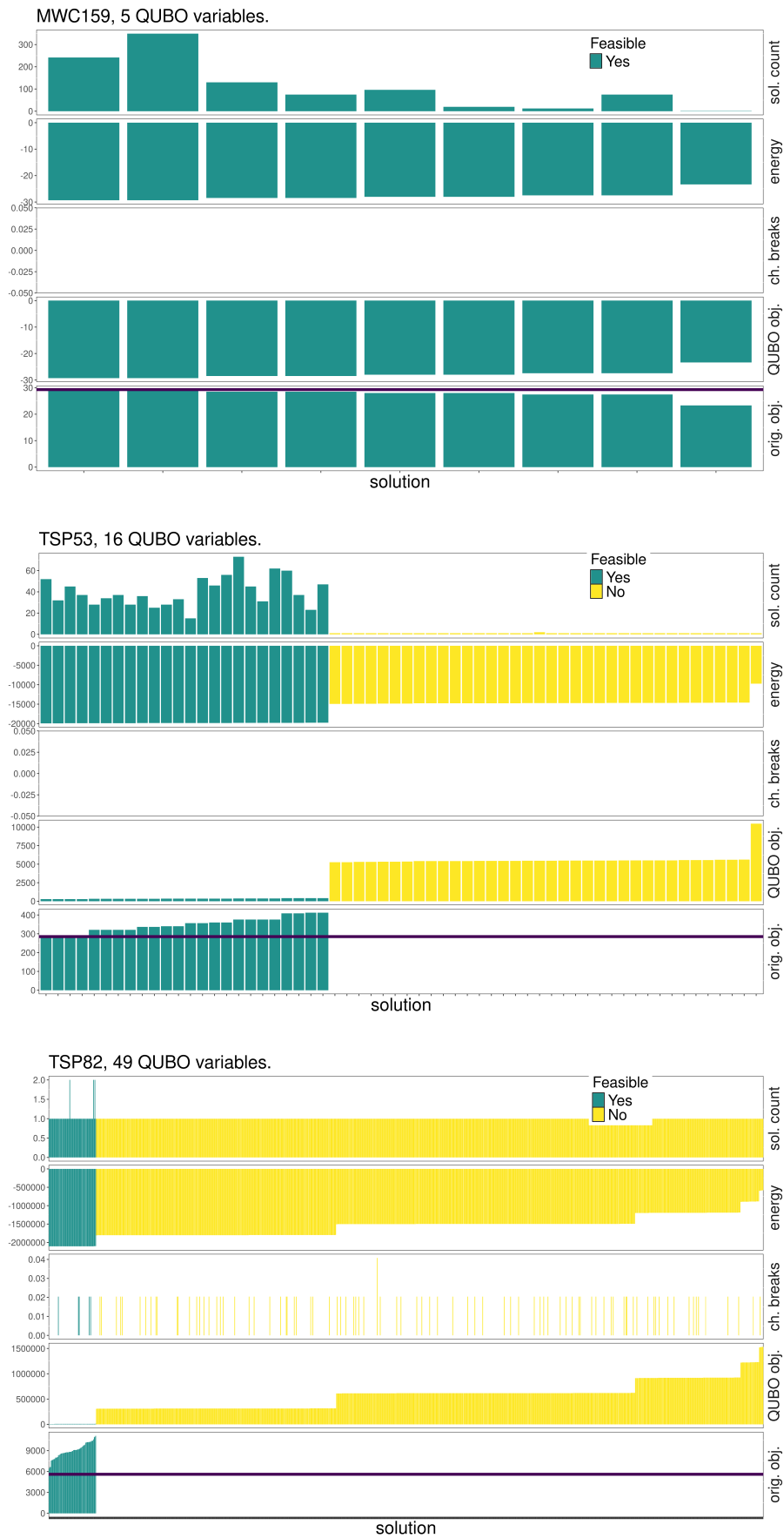


Figure 12: Final sample for three selected instances, experiment on DWave’s “Advantage” machine. Dark color marks feasible solutions.

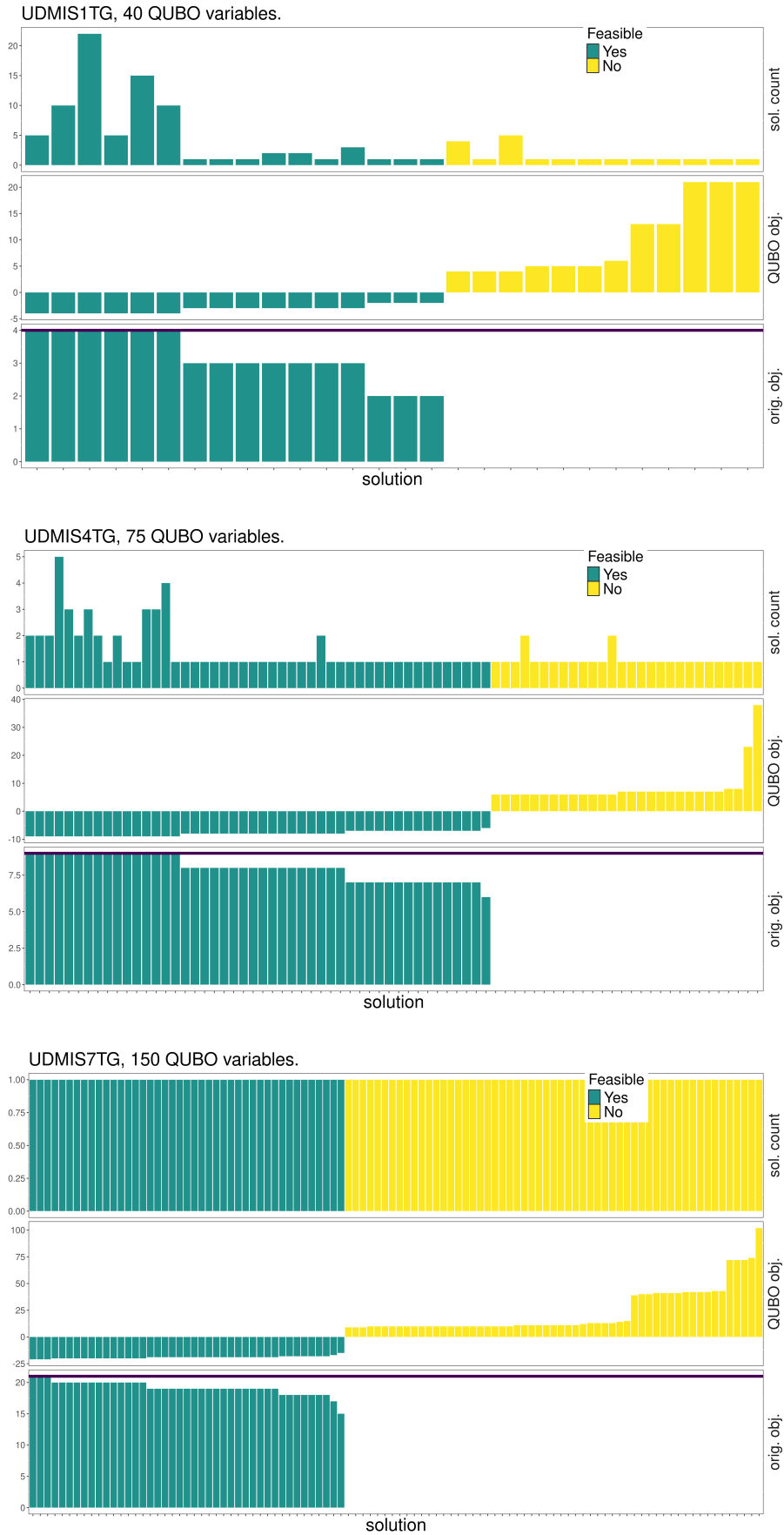


Figure 13: Final sample for three selected instances, experiment on QuEra’s “Aquila” machine. Dark color marks feasible solutions.



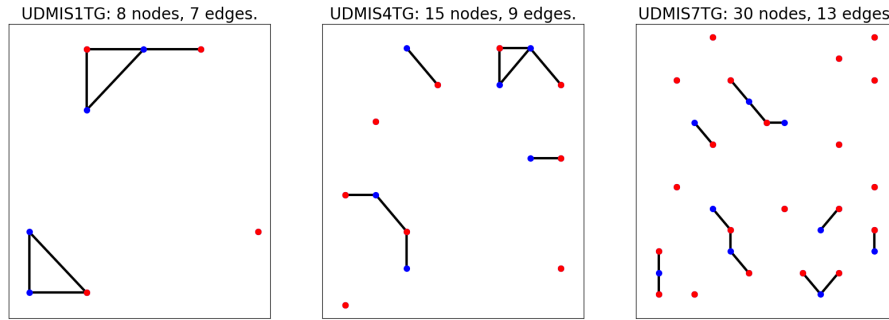


Figure 14: Selected instances solved on the *QuEra* device. Original MIS graphs, colored points represent an optimal solution.



Figure 15: Final sample for three selected instances, experiment on the *IBM qasm* simulator (left) and *nazca* quantum device (right). Dark color marks feasible solutions.

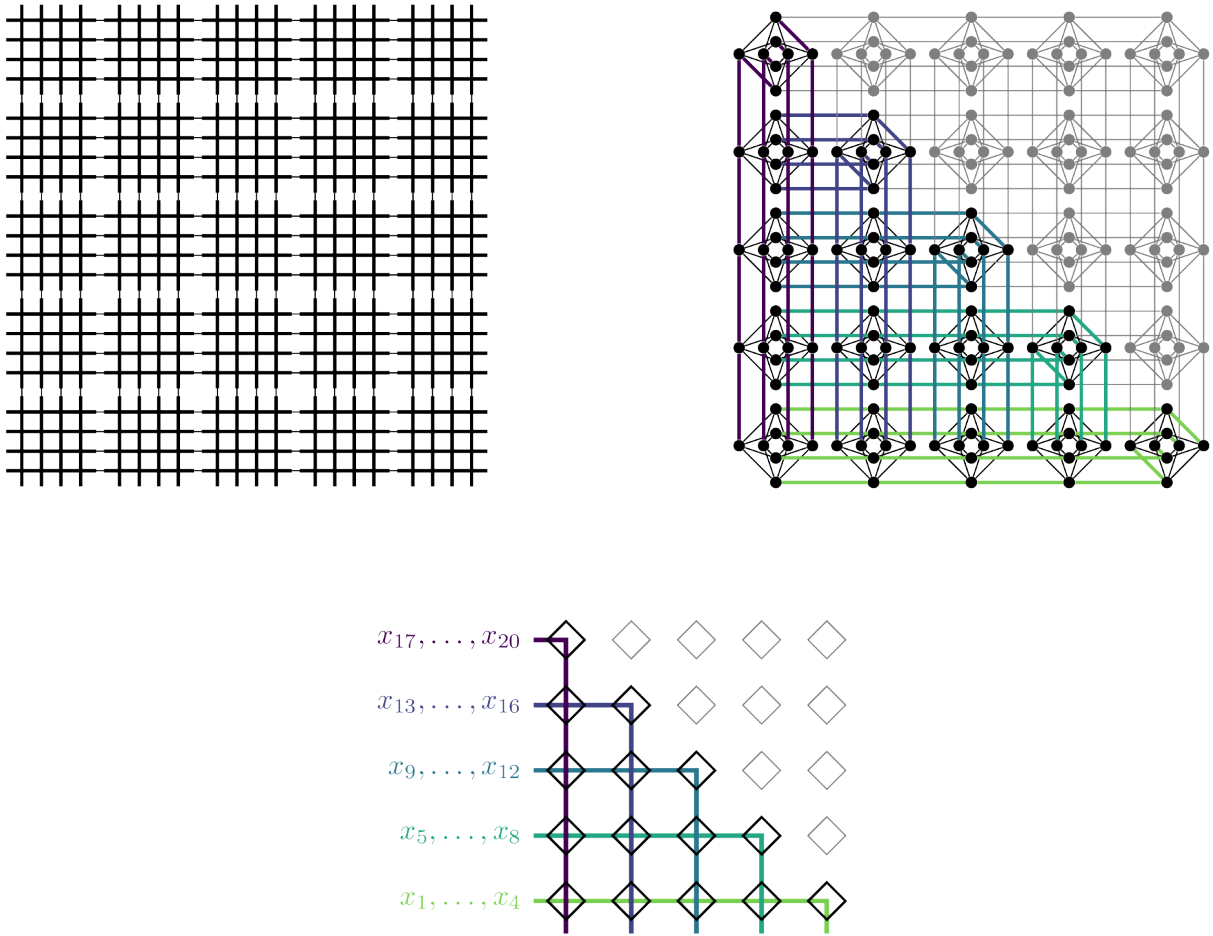


Figure 16: *D-Wave's* Chimera topology: segments corresponding to superconducting loops (top left) and their intersection graph, the Chimera graph (top right); groups used in embedding of  $K_{20}$  represented by colors; high-level logic of clique embedding (bottom) and explicit embedding (top right).

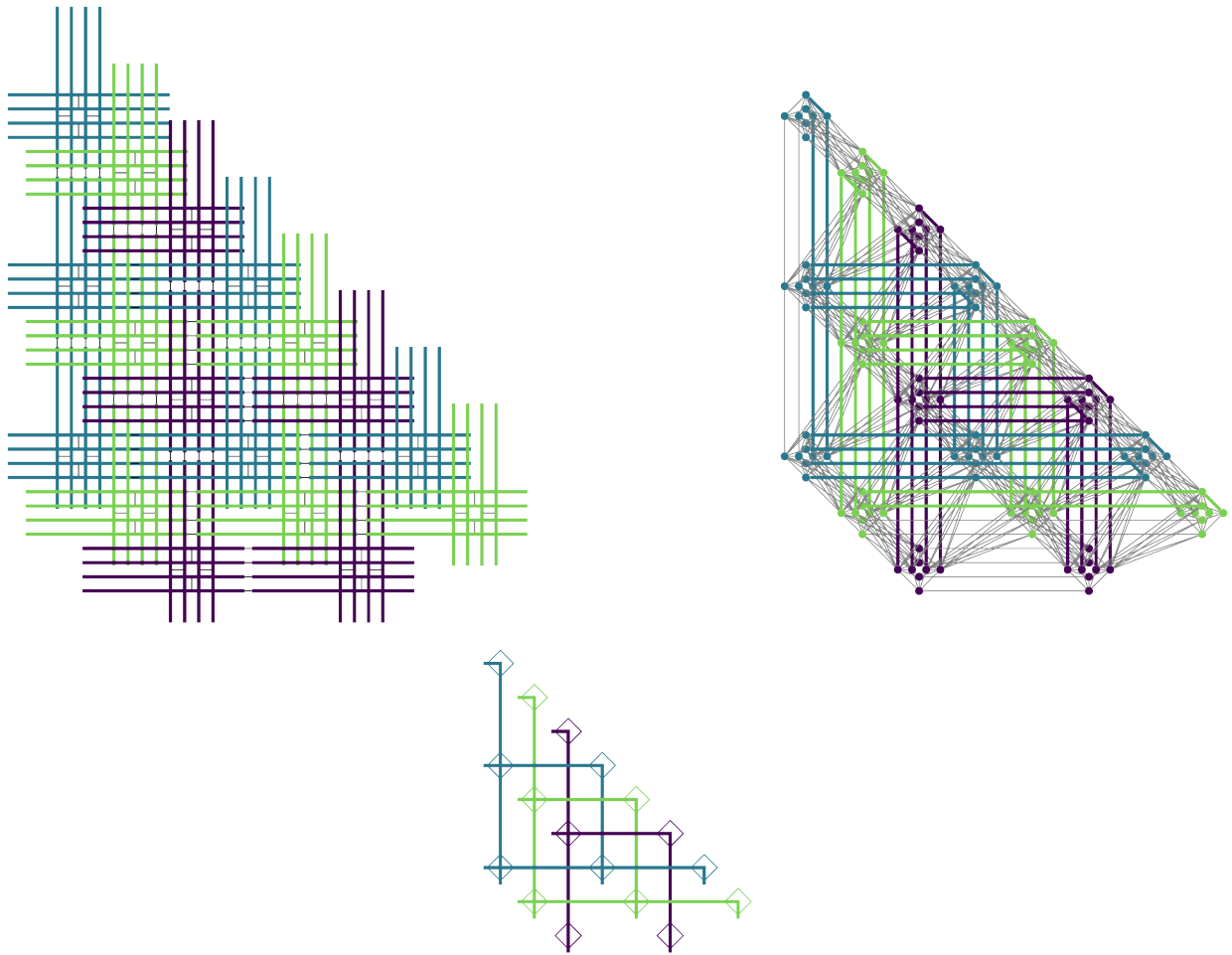


Figure 17: Section of *D-Wave's* Pegasus topology: segments corresponding to superconducting loops (top left) and their intersection graph (top right), colors representing the three Chimera subgraphs. In the clique embedding, only intersections of chain groups of the same color are realized by  $K_{4,4}$  cells; the others are realized by additional edges (bottom). Embedding of  $K_{28}$  (top right, thick colored lines).

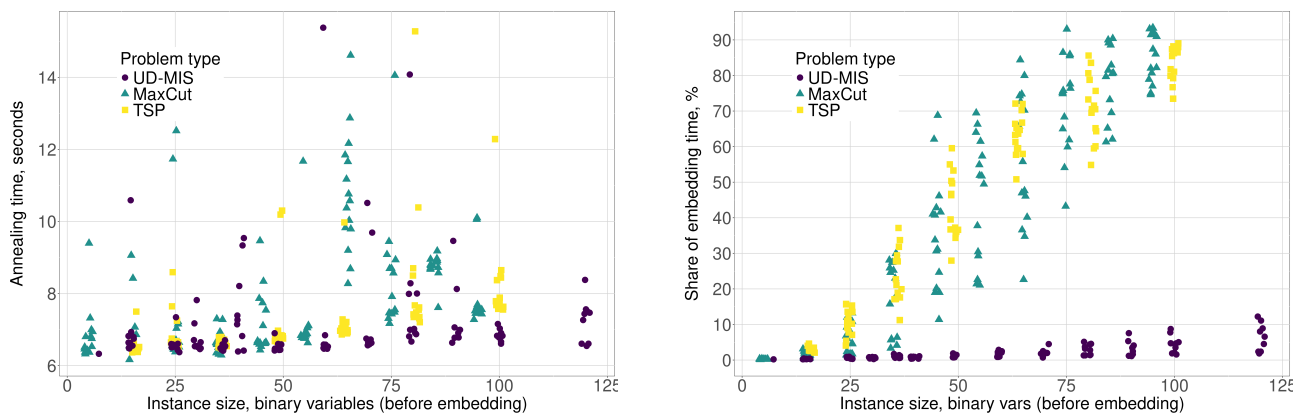


Figure 18: Annealing time (left) and the share of embedding time in the total runtime (right).